UNLV | UNIVERSITY LIBRARIES

UNLV Retrospective Theses & Dissertations

1-1-2004

Thermal analysis of a concentrating photovoltaic receiver

Isaac Mahderekal
University of Nevada, Las Vegas

Follow this and additional works at: https://digitalscholarship.unlv.edu/rtds

Repository Citation

Mahderekal, Isaac, "Thermal analysis of a concentrating photovoltaic receiver" (2004). *UNLV Retrospective Theses & Dissertations*. 1669.
http://dx.doi.org/10.25669/jeve-ntnf

This Thesis is protected by copyright and/or related rights. It has been brought to you by Digital Scholarship@UNLV with permission from the rights-holder(s). You are free to use this Thesis in any way that is permitted by the copyright and related rights legislation that applies to your use. For other uses you need to obtain permission from the rights-holder(s) directly, unless additional rights are indicated by a Creative Commons license in the record and/or on the work itself.

This Thesis has been accepted for inclusion in UNLV Retrospective Theses & Dissertations by an authorized administrator of Digital Scholarship@UNLV. For more information, please contact digitalscholarship@unlv.edu.

NOTE TO USERS

This reproduction is the best copy available.

UMI®

Reproduced with permission of the copyright owner. Further reproduction prohibited without permission.

Reproduced with permission of the copyright owner. Further reproduction prohibited without permission.

THERMAL ANALYSIS OF A CONCENTRATING PHOTOVOLTAIC RECEIVER

by

Isaac Mahderekal
Bachelor of Science
University of Nevada, Las Vegas
2002

Master of Science
University of Nevada, Las Vegas
2004

A thesis submitted in partial fulfillment
of the requirements for the

Master of Science Degree in Mechanical Engineering
Department of Mechanical Engineering
Howard R. Hughes College of Engineering

Graduate College
University of Nevada, Las Vegas
May 2004

Reproduced with permission of the copyright owner. Further reproduction prohibited without permission.

UMI Number: 1422802

INFORMATION TO USERS

The quality of this reproduction is dependent upon the quality of the copy submitted. Broken or indistinct print, colored or poor quality illustrations and photographs, print bleed-through, substandard margins, and improper alignment can adversely affect reproduction.

In the unlikely event that the author did not send a complete manuscript and there are missing pages, these will be noted. Also, if unauthorized copyright material had to be removed, a note will indicate the deletion.

UMI®

UMI Microform 1422802

Copyright 2004 by ProQuest Information and Learning Company.

All rights reserved. This microform edition is protected against unauthorized copying under Title 17, United States Code.

ProQuest Information and Learning Company
300 North Zeeb Road
P.O. Box 1346
Ann Arbor, MI 48106-1346

Reproduced with permission of the copyright owner. Further reproduction prohibited without permission.

UNLV
UNIVERSITY OF NEVADA LAS VEGAS

Thesis Approval

The Graduate College
University of Nevada, Las Vegas

April 1, 2004

The Thesis prepared by

Isaac Mahderekal

Entitled

Thermal Analysis of a Concentrating Photovoltaic Receiver.

is approved in partial fulfillment of the requirements for the degree of

Master of Science in Mechanical Engineering

Examination Committee Chair

Dean of the Graduate College

Examination Committee Member

Examination Committee Member

Graduate College Faculty Representative

Reproduced with permission of the copyright owner. Further reproduction prohibited without permission.

ABSTRACT

Thermal Analysis of a Concentrating Photovoltaic Receiver

by

Isaac Mahderekal

Dr. Robert F. Boehm, Examination Committee Chair
Professor of Mechanical Engineering
University of Nevada, Las Vegas

This paper presents the theoretical and computational analysis for a photovoltaic (PV) receiver for the Science Applications International Corporation (SAIC) dish concentrator. During photovoltaic energy conversion, thermal energy is also generated which results in increases in cell temperature. However, as the cell temperature increases, the efficiency of the PV cells drops—a 40°C increase in temperature for this unit cuts performance by 25%. An algorithm has been developed to predict the maximum cell temperature and working fluid temperature as a function of channel size, mass flow rate, cooling configuration, fluid-to-tube heat transfer coefficient and other parameters. To evaluate the transient characteristics of the system, a dynamic model of the concentrating PV collector has been developed. The model describes the change in temperature of the cells and the coolant in the receiver as a function of time, taking into account the: solar insolation, change in energy content of the element, energy transfer by the fluid flow, and temperature dependent energy flow between the element and the surroundings. Five energy balance differential equations have been solved simultaneously to examine the transient nature of the system. Computational fluid

Reproduced with permission of the copyright owner. Further reproduction prohibited without permission.

dynamics flow modeling (CFD) software has also been utilized to compare the temperature distribution along the module with the analytical results. The flow model is built and applied mesh using the preprocessing tool, GAMBIT, and the CFD analysis has been done by using Fluent. The model quantifies temperature, velocity and pressure profiles of the module.

Reproduced with permission of the copyright owner. Further reproduction prohibited without permission.

TABLE OF CONTENTS

Reproduced with permission of the copyright owner. Further reproduction prohibited without permission.

LIST OF FIGURES

Reproduced with permission of the copyright owner. Further reproduction prohibited without permission.

LIST OF TABLES

Reproduced with permission of the copyright owner. Further reproduction prohibited without permission.

ACKNOWLEDGMENTS

I would like to thank Dr. Robert F. Boehm who not only served as my academic advisor but also encouraged and patiently guided me through the thesis process and throughout my academic program. I enjoyed working with him.

I would also like to thank the following people for serving as my committee members: Dr. Bingmei M. Fu, Dr. Eugene McGaugh, and Dr. Woosoon Yim. Thank you for your time and assistance with my thesis.

The support of this work by the National Renewable Energy Laboratory is very much appreciated.

Last but not least, I would like to thank my family and friends. This work could not have been possible without their love and support.

Reproduced with permission of the copyright owner. Further reproduction prohibited without permission.

CHAPTER 1

INTRODUCTION

Purpose of the Study

An SAIC dish-Stirling solar power system was installed at UNLV in 2001. In 2003 work began to convert the unit to a dish-PV system. New fixed-focal-length facets have been installed to replace the stretched membrane facets originally on the system. A PV receiver and heat rejection system is being designed to replace the original Stirling engine. It is anticipated that the triple junction cells will be used, but the current design involves high-flux single-junction cells.

Some parts of the investigation of the receiver part of the SAIC dish are described in this paper. The cooling system consisting of several automotive radiators, a fan, and a pumped liquid coolant loop will be analyzed independently. After both cases are investigated and analyzed separately, they will be coupled and optimized.

The receiver consists of identical modules that have integral cooling connections so that modules may be arrayed in any desired arrangement. The modules are rectangular and approximately 5cm by 27cm in size. For the SAIC dish concentrator, the full receiver consists of 24 modules assembled into a flat, approximately square receiver with an aperture approximately 55cm by 60cm in size. As shown in Figure 1, the modules are arranged in a 2x12 array.

Reproduced with permission of the copyright owner. Further reproduction prohibited without permission.

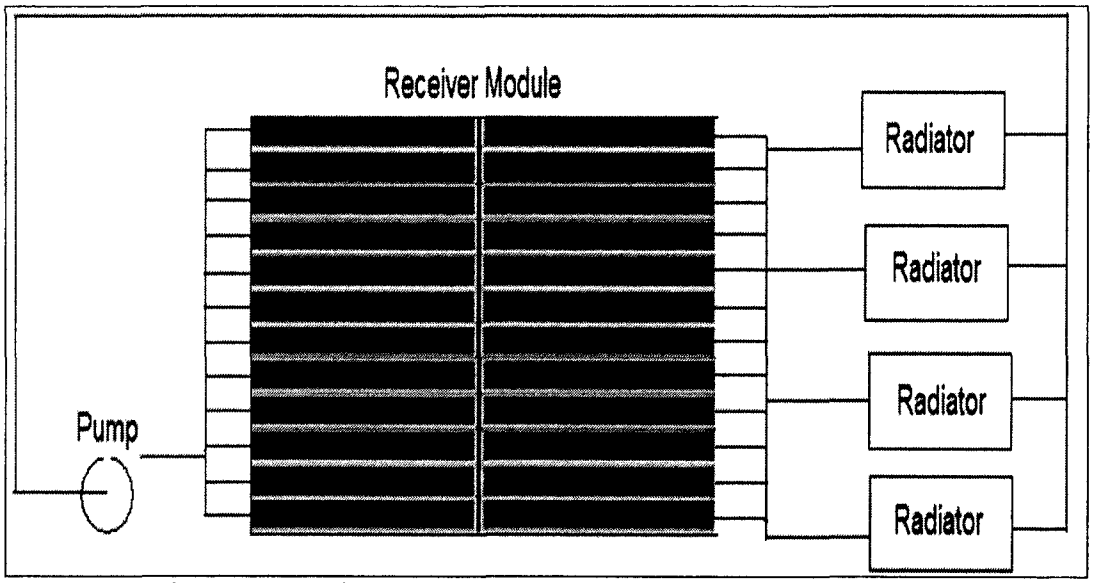

Figure 1 Receiver with 24 modules arranged in a 2x12 array.

The dish system is designed to provide a uniform flux of about 250 suns over that receiver area using a secondary concentrator. Each module consists of a substrate covered with PV cells, cooling passages behind the substrate, and module electrical and cooling flow connections on one end of the module. The module is expected to operate under uniform insolation.

Significance of the Study

Solar energy is a valuable form of energy, which has the potential to meet a significant proportion of world's energy needs. One of the major applications of solar energy is solar photovoltaic system. Concentrating photovoltaic receivers are characterized for their good reliability, higher efficiency, and low cost at moderate production levels. A recent review by the National Renewable Energy Laboratory clearly described the potential advantages (e.g., lower cost, higher efficiency, materials availability, manufacturing scale-up) of concentrating photovoltaic system over flat plate

Reproduced with permission of the copyright owner. Further reproduction prohibited without permission.

systems. Photovoltaic cells (PV) produce electricity directly from solar energy. During photovoltaic energy conversion, thermal energy is also generated which results in increases in cell temperature. However, as the cell temperature increases, the efficiency of the PV cells drops. The main goal of the study is to develop steady state and transient simulation models to predict cell temperatures and eventually optimize performance.

The absorber of the PV collector under investigation consists of an array of solar cells for generation of electricity, while fluid circulating past the absorber provides cooling. Concentrated solar energy is incident on the cells from a parabolic dish reflector. A steady state condition will be investigated to have an understanding of the temperature distribution that exists in the PV cells. Energy balance equations will be derived for various components of the system. An algorithm will also be developed to predict the maximum cell temperature and working fluid temperature as a function of mass flow rate, cooling configuration, wind- and fluid-to-tube heat transfer coefficients and other parameters. Based on the developed analysis, performance of the system as a function of system design parameters will be presented and discussed.

The second part of the study is to evaluate a transient nature of the system. Solar energy system is inherently transient. A dynamic model of the concentrating PV collector will be developed. The model will describe the change in temperature of the cells and the coolant in the receiver as a function of time, taking into account: the solar insolation, the change in energy content of the element, the energy transfer by the fluid flow, the temperature dependent energy flow between the element and the surroundings.

Reproduced with permission of the copyright owner. Further reproduction prohibited without permission.

Module Specification

In the present investigation, a solid copper plate is grooved into several rectangular passages and welded at the bottom with the flat copper plate. This will allow a direct contact between the wall and the circulating cooling fluid. The PV cells will be the typical single junction type, but designed to tolerate the high fluxes of the concentrated beam. The receiver consists of identical modules that have integral cooling connections so that modules may be arrayed in any desired arrangement. The modules are rectangular and approximately 5cm by 27cm in size. The dish concentrator system is designed to provide a uniform flux of about 250 suns over that receiver area. Each module consists of a substrate covered with PV cells, cooling passages behind the substrate, and module electrical and cooling flow connections on one end of the module. The module is expected to operate under uniform insolation.

Table 1 shows the conditions under which the module is designed to operate. This will result in the rated performance given by SAIC specifications for a PV receiver and inverter system for the SAIC dish concentrator [1]. Also included are the specifications of the expected performance under those conditions. Amonix single junction PV cells are applied in this initial design.

Table 1 Module specifications and expected performance

Module size	Rectangular, 5.1cm by 29 cm
Aperture size	Rectangular, 5 cm by 27 cm
Type of Photovoltaic Cell	Single-crystal, back-contact Silicon
Insolation at Receiver surface	1000 W/m^2 and 250 suns 250 kW/m^2
Average Cell Temperature	65°C
Cooling Flow (Maximum)	~60 gpm
Design Efficiency	~16%

Reproduced with permission of the copyright owner. Further reproduction prohibited without permission.

The temperature dependence of Amonix cell efficiency has been reported [2,3]. Among the information provided is a plot of the results of temperature sensitivity of the cells at various temperatures. See Figure 2.

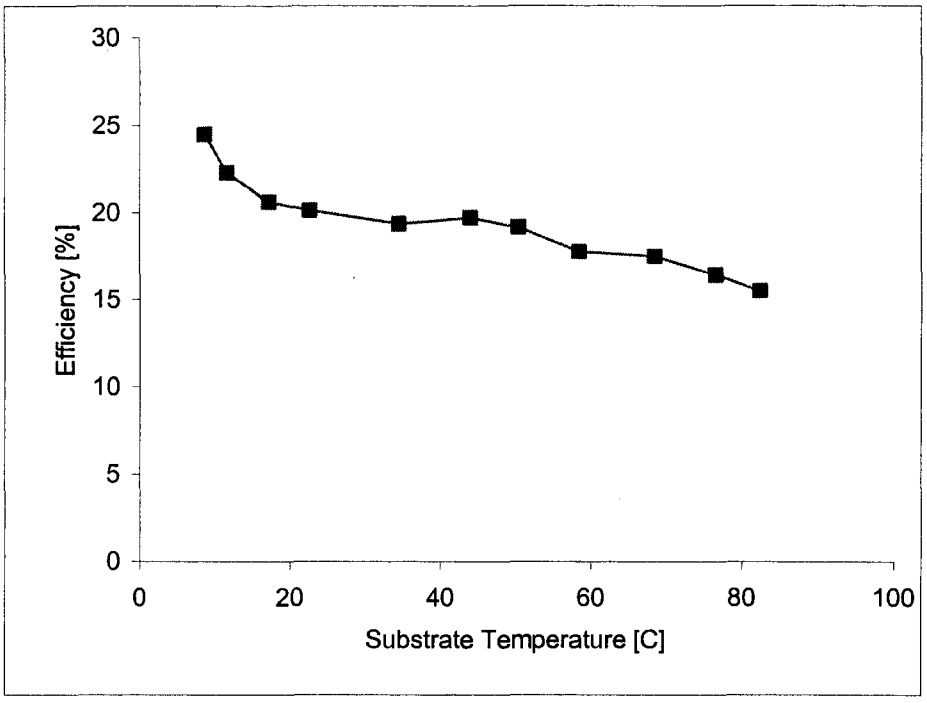

Figure 2 Efficiency of AMNX 1805 as a function of temperature

Reproduced with permission of the copyright owner. Further reproduction prohibited without permission.

CHAPTER 2

REVIEW OF RELATED LITERATURE

The starting point of this study is based on temperature and heat flux dependence of photovoltaic solar cells and their power output. The temperature dependence of Amonix cell and efficiency has been reviewed [2,3]. The paper reports the measurement results of temperature sensitivity of the cells at various temperatures. The paper presents analytical and experimental results. According to the published results, lowering the normal operating temperature of the system increases the power output for both applications: flat plate and concentrated cases. The author also stated that a solar cell with a certain photovoltaic power conversion efficiency at one-sun would have a higher conversion efficiency if operated at higher concentration at the same temperature. The reason for this increase in efficiency is due to the increase in open-circuit voltage due to increased light generated current. It is apparent, for concentrated systems, approximately by the number of suns times the residual heat must be dissipated through the same cell area compared to one-sun applications. The paper demonstrates the relationship of temperature and the open-circuit voltage (V_{OC}) and the temperature sensitivity of V_{OC} can be obtained by differentiating the V_{OC}. To validate the analytical approach an experimental is done. Results of experiment of a typical Amonix cell shown to define the temperature sensitivity of Voc at various temperatures and

Reproduced with permission of the copyright owner. Further reproduction prohibited without permission.

concentrations. For the temperature range tested, all cell parameters showed a linear behavior for their efficiency and V_{OC} [2].

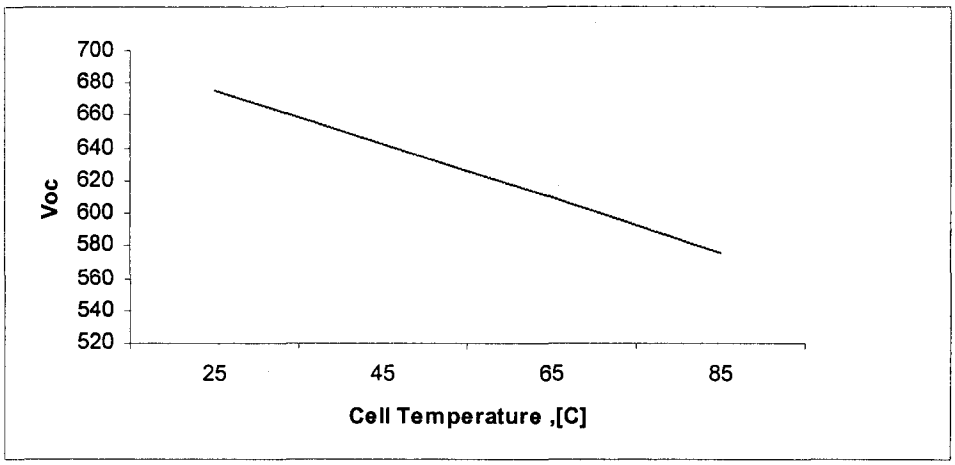

Figure 3 Open circuit voltage of AMNX 1805 as function of temperature

After reviewing the analysis, concentrated applications of the same cell would produce power more efficiently. For a 250 suns concentrator application, the cell would be approximately 20% more efficient than one-sun applications. However, approximately 80% of the residual heat has to be rejected.

There are few reports in literature related to work on thermal analysis of a concentrating receiver. A few theoretical as well as experimental studies [9,10] have been made on the concentrated PV systems. They carried out experimental studies on combined photovoltaic/thermal air and liquid heating system. They also presented a steady state model for performance prediction.

Conventry [9] simulated photovoltaic/thermal collector using TRNSYS component (type 262). The combined heat and power solar collector developed at Australian National University is a photovoltaic/thermal collector utilizing parabolic mirrors to concentrate light by a factor of 25-35x. The paper presents some measured results for

Reproduced with permission of the copyright owner. Further reproduction prohibited without permission.

thermal and electrical output from the collector, as well as an overview of major components.

Garg and Adhikari [10] presented a study on the performance of a hybrid pv/thermal collector. In the steady state analysis they assumed the solar cell efficiency by a linear decreasing function of its temperature. Based on heat transfer analysis they developed energy balance equations and predicted performance.

The above mentioned and related literature has mostly dealt with flat plate collectors or concentrated with a low amount heat to be rejected. Studies on the transient nature of the system are very limited and the temperature is assumed to be constant through out the module. In the present investigation 250000 W/m^2 of flux is applied on a 60 by 56 cm surface area of collector. The dish concentrator system is designed to provide a uniform flux of about 250 suns (number of sun concentration) over that receiver area. More than 80% of the heat has to be rejected to keep the cell temperature in a good operating condition. Different geometries and parameters had to be investigated and tested to get the desired cell temperature.

Reproduced with permission of the copyright owner. Further reproduction prohibited without permission.

CHAPTER 3

THEORETICAL ANALYSIS AND RESULTS

The system under investigation is shown in Figure 4.

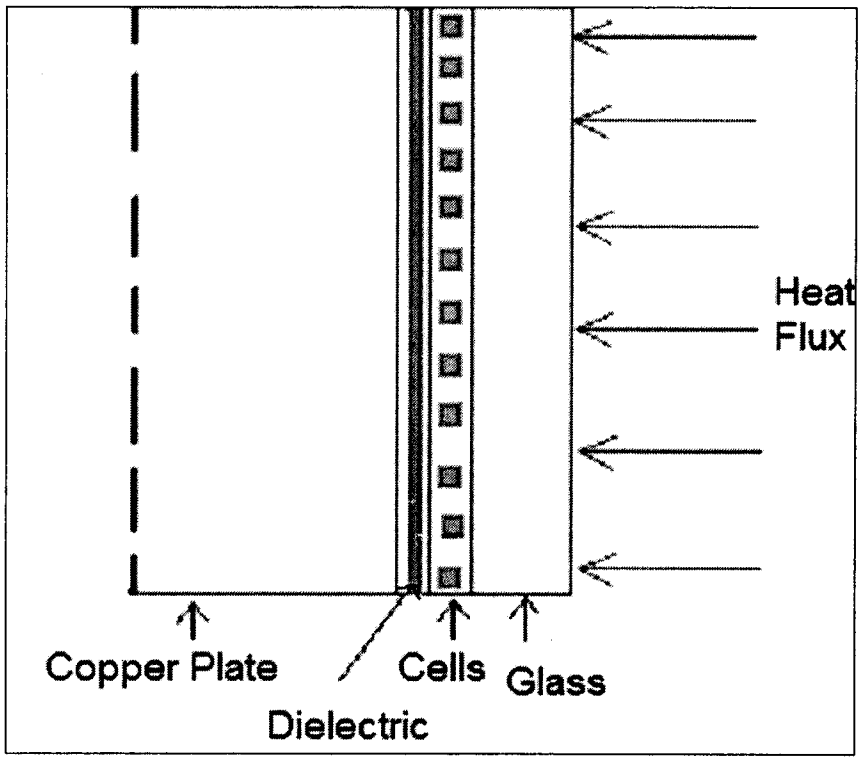

Figure 4 Cross sectional view of the system

The absorber of the PV collector under investigation consists of an array of solar cells facing the beam and fluid circulating through the back of the absorber to provide cooling. Concentrated solar energy is incident on the cells from a parabolic dish reflector. The system consists of protective glass, solar cells pasted over dielectric material, and a grooved copper plate absorber. It is assumed the 250,000 W/m^2 is the

Reproduced with permission of the copyright owner. Further reproduction prohibited without permission.

effective flux (the amount of total heat flux absorbed by the solar cells). Low thermal conductivity and low electrical conductivity characterize the dielectric material used for electrically isolating the solar cells.

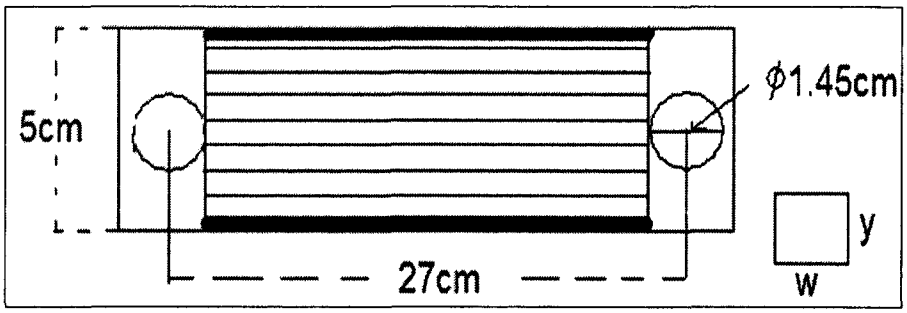

Figure 5 Module cooling plate configuration and dimensions

Weather Data Manipulation and Thermal Losses

At some typical location on the solar cell where the temperature is Tcell, solar energy of amount S is absorbed by the plate, where S equals the incident solar radiation reduced by the optical losses. This absorbed energy is distributed to thermal losses and to useful electric power. The energy loss through the top is the result of convection and radiation between the glass and the solar cells. The procedure for solving for the top loss coefficient is an iterative process. First a guess is made of unknown cover temperatures, from which the convective and radiative heat transfer coefficients between parallel surfaces are calculated. With these estimates the top loss coefficient can be solved. The process is repeated until the cover temperatures do not change significantly between successive iterations.

To estimate the solar flux for Las Vegas the Typical Meteorological Year (TMY) data published by National Renewable Energy Laboratory (NREL) are used. The TMYs

Reproduced with permission of the copyright owner. Further reproduction prohibited without permission.

are data sets of hourly values of solar radiation and meteorological elements for a 1-year period. The data files for the typical meteorological year (TMY) data sets were derived from the 1961-1990 National Solar Radiation Data Base (NSRDB). Figure 6 shows the available solar energy to be absorbed by the cells of five months (May to September). This energy is multiplied by 250-concentration factor to get the desired higher flux.

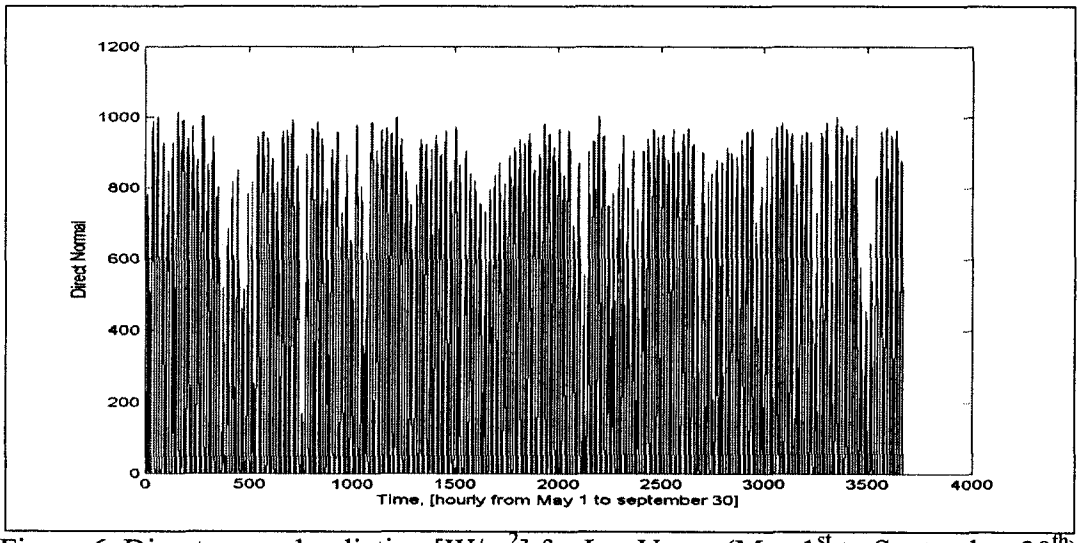

Figure 6 Direct normal radiation [W/m^2] for Las Vegas (May 1st to September 30th)

Based on the TMY data and neglecting the optical losses or gains, a 1000 watt/m^2 energy rate is assumed in the rest of the analysis. The analytical and the computational results are based on the assumption of 1000 Watt/m^2 and 250 suns (250000 Watt/m^2) on the 5 by 27 cm^2 surface area of the module.

One Dimensional Steady State Model

This model assumes that the absorbed incident solar radiation not converted to electricity is converted to thermal energy at the cell. This thermal energy is conveyed to the surfaces by conduction and removed by convection: either to the cooling water on

Reproduced with permission of the copyright owner. Further reproduction prohibited without permission.

the back or to ambient off of the front. The thermal network of the system is shown in Figure 7.

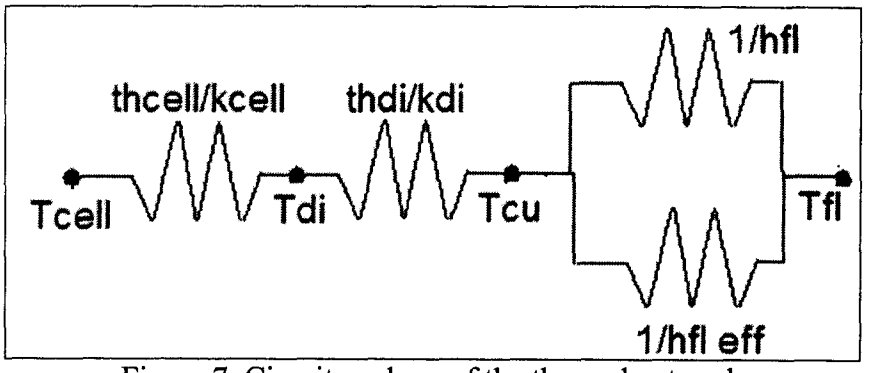

Figure 7 Circuit analogy of the thermal network

The following assumptions have been made to simplify the analysis:

1 Steady state energy transfer has been achieved.

2 Side losses from the system are negligible.

3 The inlet water temperature is constant at 315K

4 The total heat to be rejected is 250 kW/m^2

Based on these assumptions, the steady-state energy-balance equations for the cell, the insulator between the solar cells and the plate, the top absorber plate, the walls of the channel and the mean temperature can be written as:

$$q''\cdot A - \alpha\cdot(Tcell - Tdi) = 0 \quad (1)$$

$$(-\alpha - \beta)\cdot T_{di} + \alpha\cdot T_{cell} + \beta\cdot T_{cu} = 0 \quad (2)$$

$$\beta\cdot(Tdi - Tcu) - \mu - 2\cdot\varepsilon\cdot(Tcu - Tribs) \quad (3)$$

$$2\cdot\varepsilon\cdot(T_{cu} - T_{ribs}) - \lambda = 0 \quad (4)$$

$$m\cdot C_{fl}\cdot(T_{in} - T_{out}) + \mu + \lambda = 0 \quad (5)$$

Reproduced with permission of the copyright owner. Further reproduction prohibited without permission.

Where:

$$\alpha = \frac{\kappa_{cell}}{th_{cell}} \cdot w \cdot z \quad , \quad \beta = \frac{\kappa_{di}}{th_{di}} \cdot w \cdot z \quad , \quad \varepsilon = \frac{\kappa_{cu} \cdot th_{fin} \cdot z}{L}$$

A linearly decreasing temperature profile is assumed along the height (y) of the passages. Where:

$$\lambda = hfl \cdot z \cdot \int_0^L \left[(Trib - Tcu) \cdot \frac{y}{L} + Tcu - T_{fl} \right] dy$$

$$\mu = h_{fl} \cdot \left(w - 2 \cdot th_{fin} \right) \cdot z \cdot \left(Tcu - T_{fl} \right)$$

The energy equations (1-5) are solved simultaneously to evaluate the temperature at each surface. Petukhov's correlation was used for computing the local Nusselt number for fully developed turbulent flow [4]. Different fin geometries are evaluated to achieve the desired cell temperature at low pump work (lower pressure drop). Considering the pump work required and the cell temperature to be achieved a mass flow rate of 0.1561 kg/sec per module (30 gpm for the whole system), depth of 3mm and fin thickness of 1mm is used to compare different channel sizes.

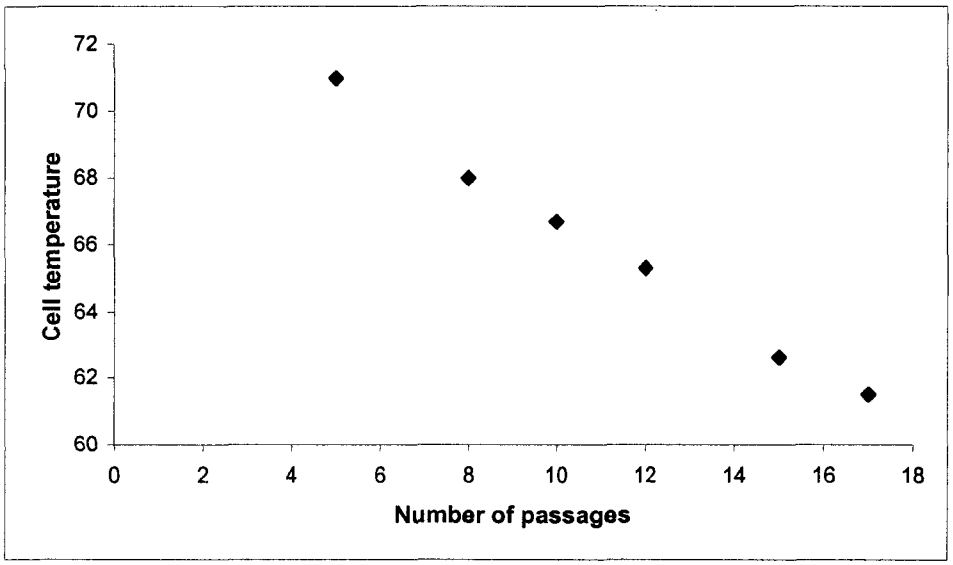

Figure 8 Number of channels versus cell temperature, [C]

Reproduced with permission of the copyright owner. Further reproduction prohibited without permission.

As shown in Figure 8, the cell temperature is 65.3°C for the case of 12-fin geometry. Therefore, to achieve a cell temperature lower than 65°C, the number of fins has to be greater than twelve. Most of the cases investigated in this paper are the 15 and 17-fin geometry since those geometries gave the desired cell temperatures (less than 65°C) of 62.7°C and 61.5°C respectively. However, as the number of passages increases, the hydraulic diameter decreases and in turn the pressure drop increases. It is also noticed that the difference in cell temperature between 15 and 17-fin geometry is 1°C but the difference in pressure drop is greater than 1250 Pa.

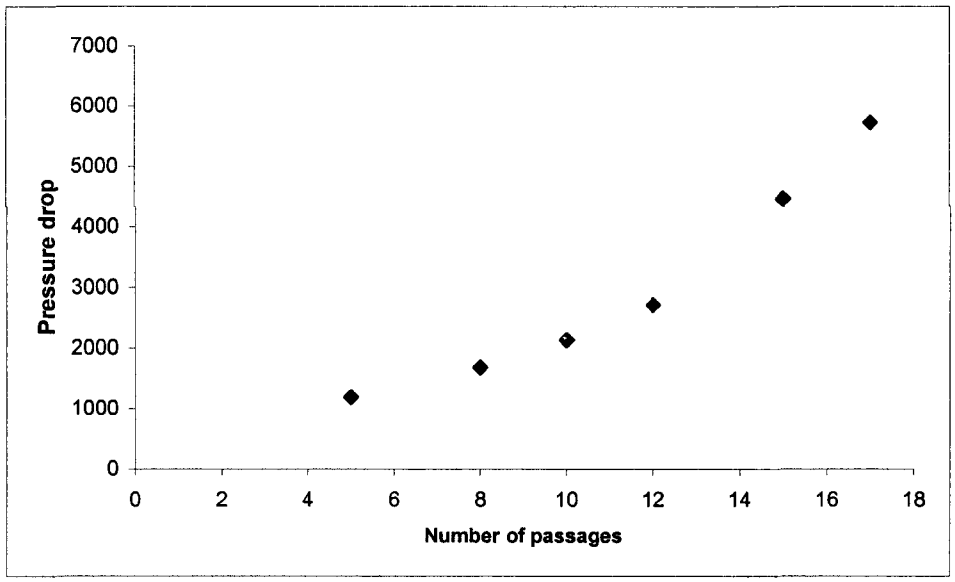

Figure 9 Number of channels versus pressure drop [Pa]

Reproduced with permission of the copyright owner. Further reproduction prohibited without permission.

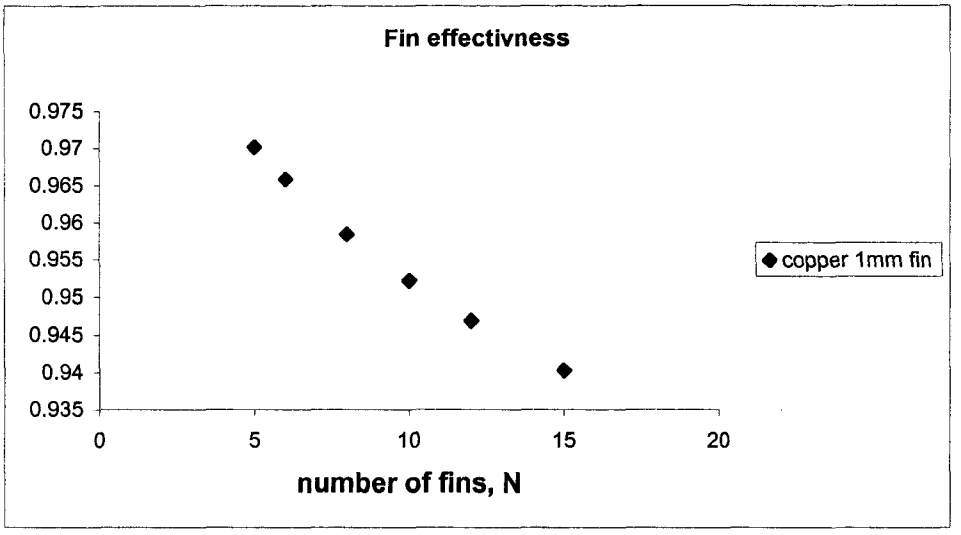

Figure 10 Fin effectiveness as function of number of fins, N

Fin effectiveness and total heat transfer rate are also assessed. The computation of the heat transfer is done as a function of number of fins (N) by fixing the fin thickness at 1mm and increasing the number of fins by reducing the spacing between the fins. The calculation for this particular case is based on an average convection coefficient associated with the flow. Parametric calculations yield the variation of fin effectiveness with N and total heat transfer rate with N as shown in Figures 10 and 11.

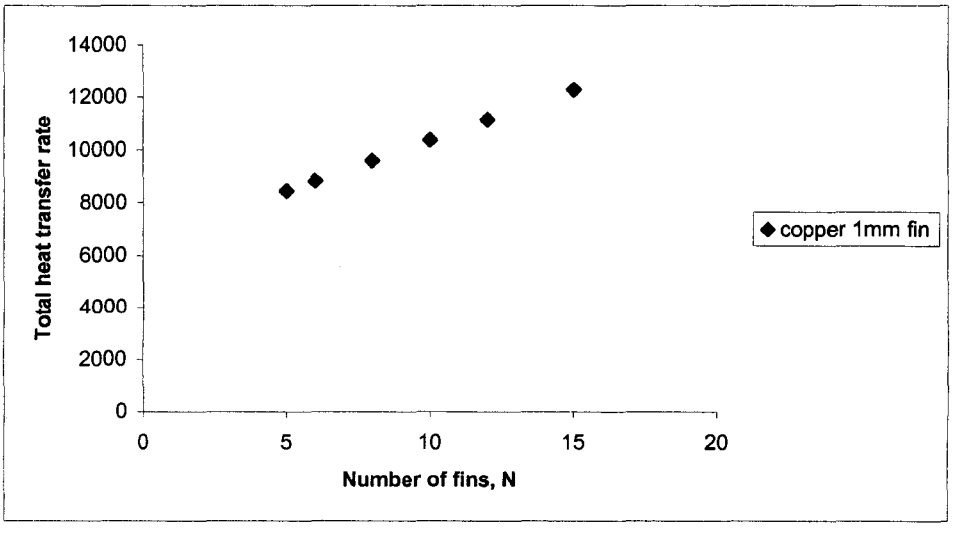

Figure 11 Heat transfer rate [W] as function of number of fins, N

Reproduced with permission of the copyright owner. Further reproduction prohibited without permission.

Temperature difference per component of the fifteen-fin geometry is shown in Table 2. Since the dielectric material is a poor heat conductor one can see the biggest change in temperature occurs across this material.

Table 2 Temperature distributions by component

	Thickness, m	Conductivity, W/m-K	Temp. °C
Tcell	0.000102	138.0	62.7
Tdi	0.000076	2.2	62.5
Tcu	0.002362	400	53.4
Trib	0.001	400	51.5
Tfl			43.6

Transient Heat Transfer Model

Two models will be discussed under this section. The first case will be evaluated by applying a time varying flux directly on the wall of the copper rectangular channel. The wall temperature and the fluid temperature will be solved as functions of time and position along the flow direction. This will result in a partial differential equation and will be solved using Laplace transforms. The use of Laplace transforms in the solution of partial differential equations is convenient and efficient for our case. The partial differential equation with the boundary and initial conditions for the fluid temperature (T(t,z)) will be transformed with respect to time. After the transformation the ordinary differential equation, a function of z with constant parameter s carried along, will be solved and finally the inverse Laplace will be applied.

The second investigation involves imposing a constant maximum flux on the solar cells. This will require solving five ordinary differential equations simultaneously. The

Reproduced with permission of the copyright owner. Further reproduction prohibited without permission.

results will demonstrate the time that is required to reach the steady state after initiation of the flux. Results are demonstrated using a fifteen-fin geometry.

Time Varying Solar Flux

The following assumption have been made to simplify the analysis:

1. Temperature varies only the flow direction of the coolant.
2. Side losses from the system are negligible.
3. The inlet coolant temperature is constant at 315K.

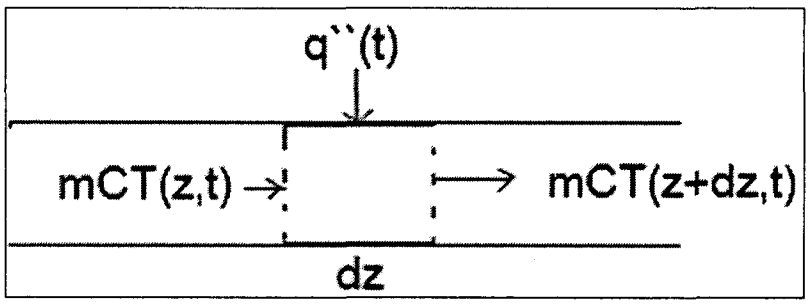

Figure 12 Energy balance on a copper channel with time varying flux.

The above energy balance yields a first order PDE written as follows.

$$-m\cdot C_{fl}\cdot T_z(t,z)\cdot dz + q''(t)\cdot w\cdot dz = \rho\cdot C_{fl}\cdot A\cdot T_t(t,z)\cdot dz \qquad (6)$$

To show a result, a flux for a good sunny day in Las Vegas is collected and averaged. The data is curve fitted using third a order polynomial and inputted into (6).

$$-mC_{fl}T_z + \left(-1\cdot 10^{-9}\cdot t^3 - .0003t^2 + 15.5t + 8619\right)\cdot w = \rho\cdot C_{fl}A\cdot T_t \qquad (7)$$

The boundary and initial conditions are:

$$T(t,0) = Tin \text{ and } T(0,z) = Tin$$

Reproduced with permission of the copyright owner. Further reproduction prohibited without permission.

When applying the Laplace transform, since the first term in the left hand side of (7) is not a function of t, the z derivatives may simply be taken out of the integral according to Leibnitz' rule [5]. The integral on the right hand side of equation (7) is integrated by parts. Applying the initial condition yields:

$$\frac{d}{dz}T(s,z) + \frac{\rho \cdot A}{m} \cdot s \cdot T(s,z) = \frac{\rho \cdot A}{m} \cdot T(0,z) + \frac{w}{m \cdot C_{fl}} \cdot q''(s) \qquad (8)$$

Where:

$$q''(s) = \left(\frac{-6 \cdot 10^{-9}}{s^4} - \frac{0.0006}{s^3} + \frac{15.507}{s^2} + \frac{86191}{s} \right)$$

This is an ordinary differential equation for T(s,z), which is considered to be a function of z with a constant parameter s carried along. The initial condition has already been incorporated into (7). The boundary condition of the original partial differential equation will be transformed to provide the boundary condition for (8). After solving the ODE, applying the inverse Laplace transform and utilizing the parameters for the fifteen-fin geometry, the temperature of the fluid as function of time and z is obtained. The wall temperature (Tcu (t, z) or Twall (t, z)) can be evaluated since the fluid temperature, T (t, z), has already been found.

$$q''(t) = h_{fl} \cdot \left(T_{cu}(t,z) - T_{fl}(t,z) \right) \qquad (9)$$

Reproduced with permission of the copyright owner. Further reproduction prohibited without permission.

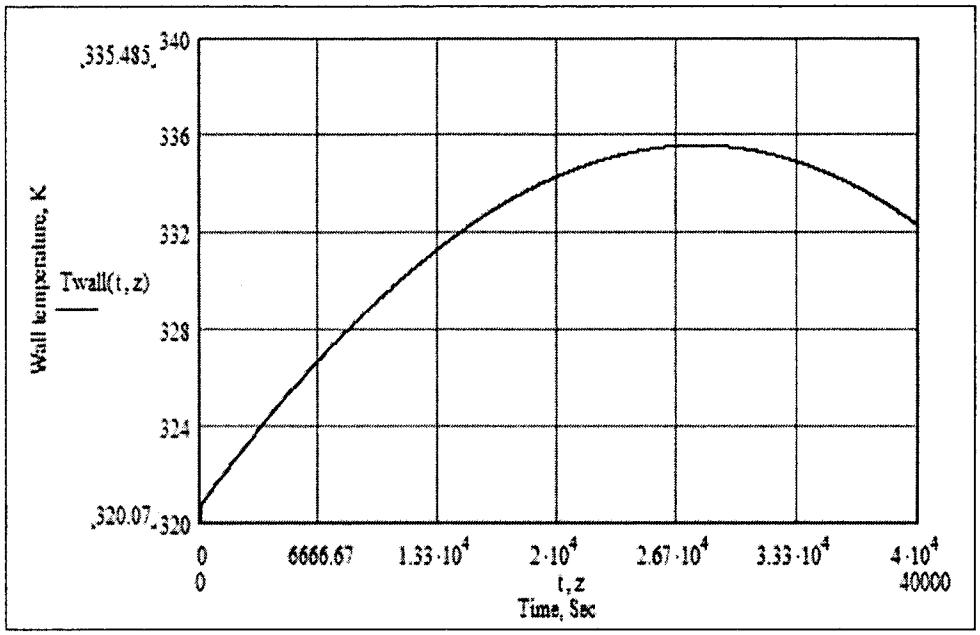

Figure 13 Temperature of the wall [K], as function of time [sec]

The temperature of the wall increases for the first seven and half hours as the flux increases. After the first seven and half-hours the flux decreases and as is the wall temperature.

Constant Heat Flux

The equations to be solved are the same as the steady state case except for the additional storage term. Laplace transform is used to evaluate the ODE. The five equations are solved simultaneously to evaluate the transient nature at each surface. The flux is applied instantaneously on the cells as shown in Figure 14. The following assumptions have been made to simplify the analysis:

1. Side losses from the system are negligible.
2. The inlet water temperature is constant at 315 K
3. The total heat to be rejected is 250 kW

Reproduced with permission of the copyright owner. Further reproduction prohibited without permission.

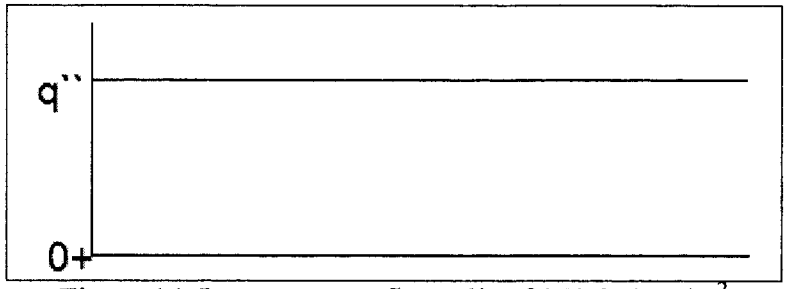

Figure 14 Instantaneous flux, q``, of 250,000 W/m^2

The initial and boundary conditions are:

$$T(z,0) = Tin \text{ and } T(0,t) = Tin$$

The five ordinary differential equations are listed below:

$$q''\cdot A - \alpha\cdot\left(T_{cell} - T_{di}\right) = \theta_{cell}\cdot\left(\frac{d}{dt}T_{cell}\right) \tag{10}$$

$$\left(-\alpha - \beta\right)\cdot T_{di} + \alpha\cdot T_{cell} + \beta\cdot T_{cu} = \theta_{di}\cdot\left(\frac{d}{dt}T_{di}\right) \tag{11}$$

$$\beta\cdot(Tdi - Tcu) - \mu - 2\cdot\varepsilon\cdot(Tcu - Tribs) = \theta_{cu}\cdot\left(\frac{d}{dt}T_{cu}\right) \tag{12}$$

$$2\cdot\varepsilon\cdot\left(T_{cu} - T_{ribs}\right) - \lambda = \theta_{ribs}\cdot\left(\frac{d}{dt}T_{ribs}\right) \tag{13}$$

$$m\cdot C_{fl}\cdot\left(T_{in} - T_{out}\right) + \mu + \lambda = \theta_{fl}\cdot\left(\frac{d}{dt}T_{fl}\right) \tag{14}$$

Where:

$$\theta = \rho\cdot V\cdot C$$

The results for cases of fifteen and seventeen fin geometries are shown in Figure 15.

Reproduced with permission of the copyright owner. Further reproduction prohibited without permission.

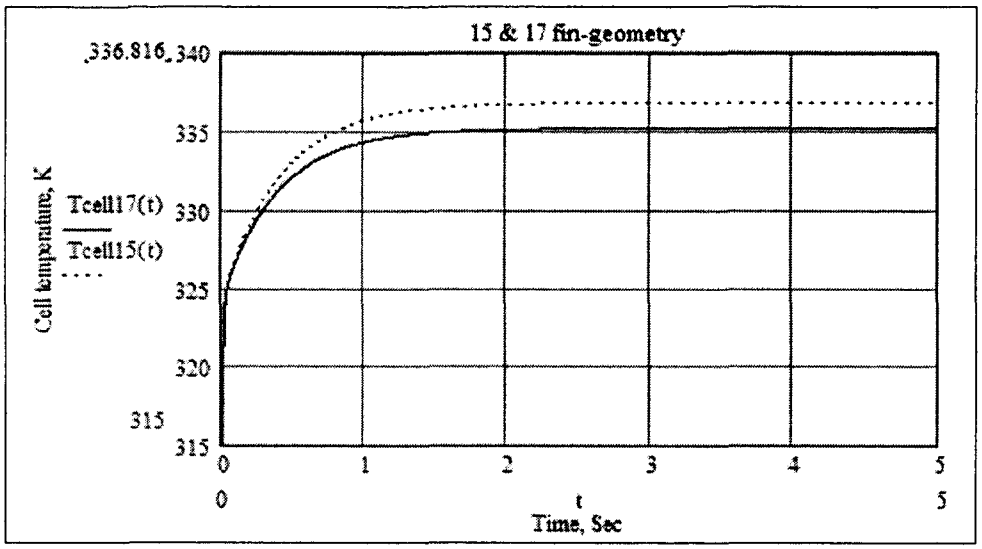

Figure 15 Cell temperature [K] for 15 and 17 fin-geometry

The steady state cell temperature difference between the two geometries is around 1.5, which is the same as in the previous steady state analysis. The time required to reach a steady state is less than two seconds for this particular case. Figures 16 and 17 demonstrate an extreme case where there is no cooling water circulating and a very slow flow rate (basically the fluid is nearly stagnant, 0.5gpm) respectively. The time elapsed to reach a temperature 500K is less than 3 seconds.

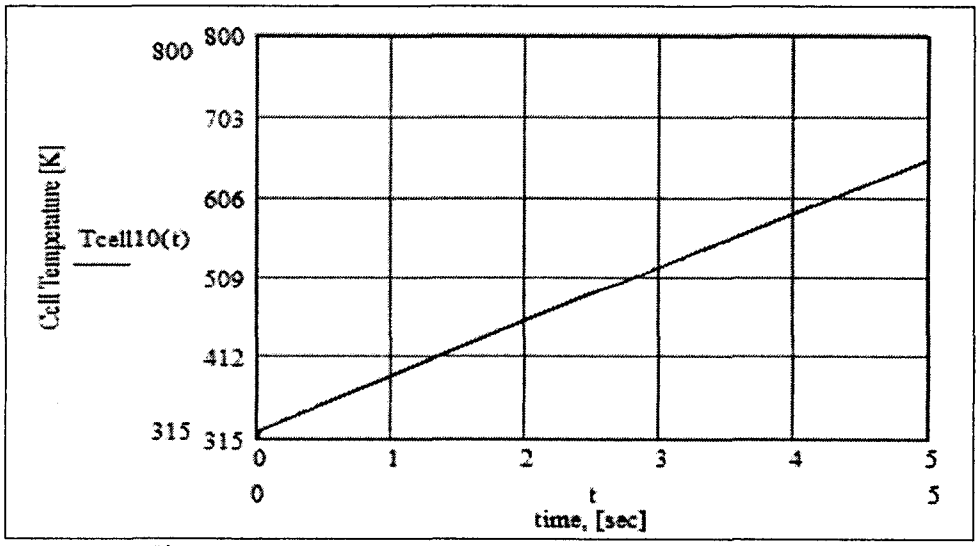

Figure 16 Cell temperature [K] without cooling fluid

Reproduced with permission of the copyright owner. Further reproduction prohibited without permission.

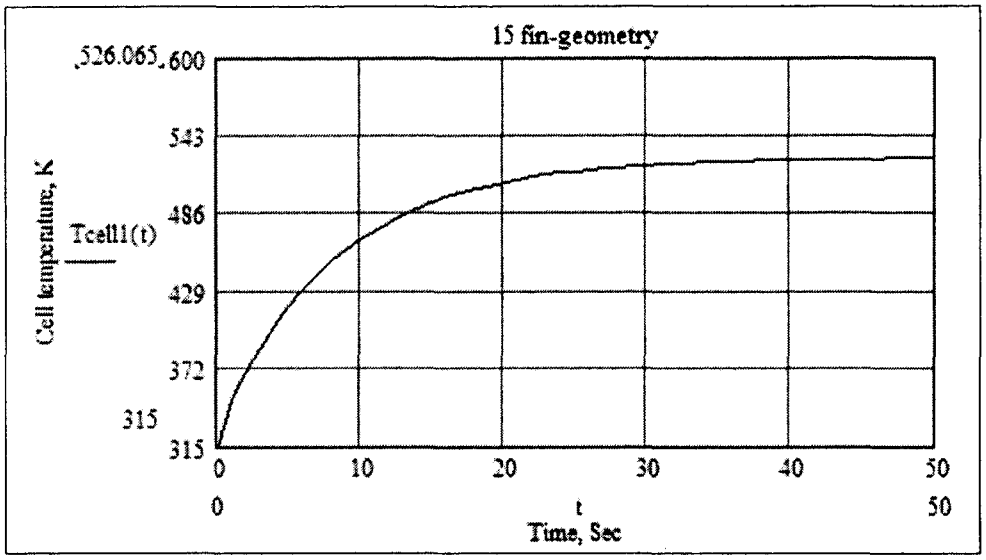

Figure 17 Cell temperatures [K] with a flow rate of 0.5 gpm for the whole system

Reproduced with permission of the copyright owner. Further reproduction prohibited without permission.

CHAPTER 4

COMPUTATIONAL FLUID DYNAMICS FLOW MODELING

We then applied a CFD model to the flow in the channels. The purpose of this was to understand details primarily of the pressure drop and the heat transfer parameters there. The temperature distribution found using CFD could then be applied to our analytical results. The flow model is built and the mesh applied using the preprocessing tool, GAMBIT. Then Fluent was used to perform the CFD analysis. The model quantifies temperature, velocity and pressure profiles of the fluid flow through the module. The model created has 373087 nodes. Fifteen flow passages are used with 2 mm by 2 mm flow area and 1mm fin and wall thickness. The inlet fluid temperature is constant at 315 K. The boundary conditions are specified as follows: a constant heat flux of 250 kW/m^2 at the top of the module and adiabatic boundary condition on both sides and the bottom. A coupled heat transfer condition is selected between the fluid and solid surface region. This is applicable only to walls that form the interface between two regions (such as the fluid/solid interface for a conjugate heat transfer problem). Standard k - epsilon turbulence model is used for the viscous model (based upon the magnitude of the Reynolds numbers). Also used in the computation were an implicit formulation, 3D model, steady time, absolute velocity formulation and cell-based gradient.

Reproduced with permission of the copyright owner. Further reproduction prohibited without permission.

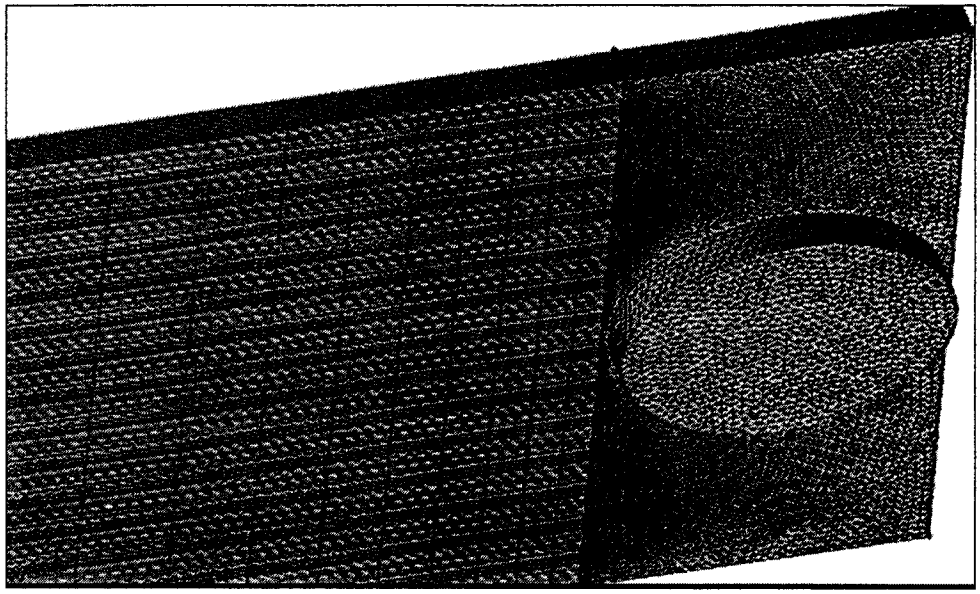

Figure 18 Applied mesh on 15 fin geometry module with pipe diameter of 1.45 cm

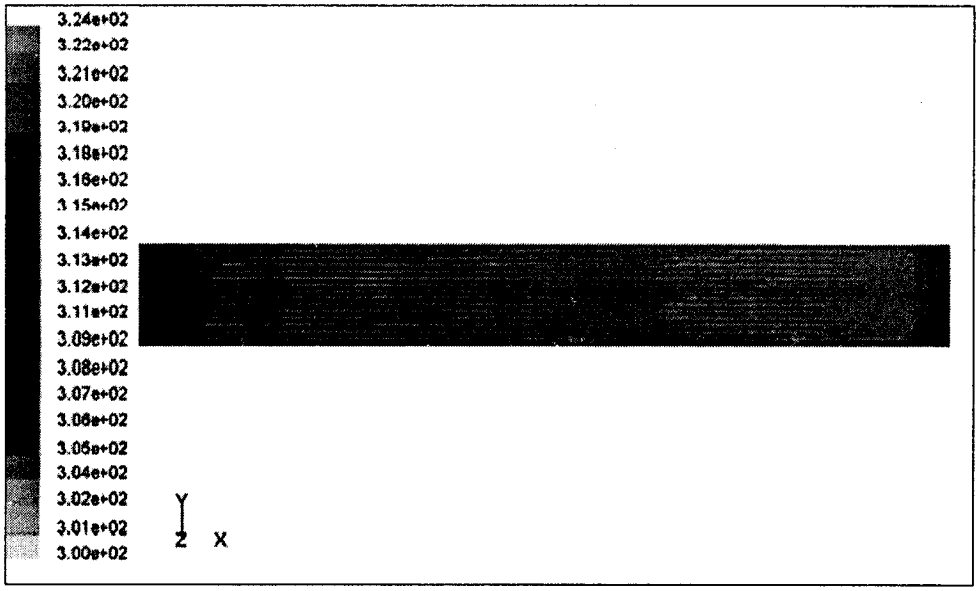

Figure 19 Contours of wall temperature [K] for flow rate of 2.5 gpm per module

Reproduced with permission of the copyright owner. Further reproduction prohibited without permission.

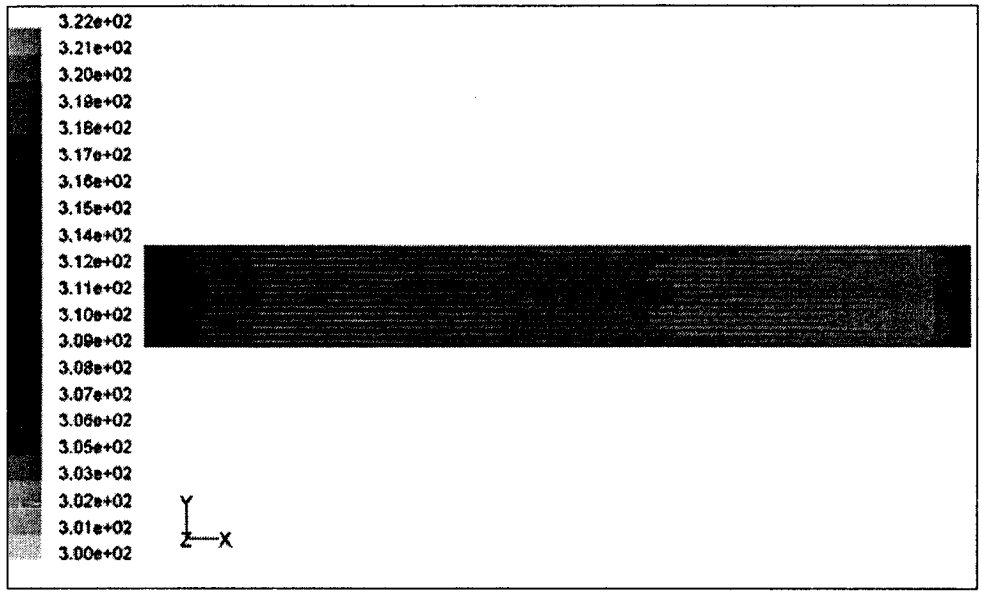

Figure 20 Contours of wall temperature [K] for flow rate of 3.00 gpm per module

The maximum module wall temperature for 2.5 and 3.0 gpm/module is 324 K and 322 K respectively is shown in Figure 19 and 20. In both cases the wall temperature increases in the flow direction and it is constant perpendicular to the flow direction. This model shows the temperature distribution on the module, which is harder to visualize using analytical method. The result closely agrees with the analytical part. Figure 21 shows the temperature distribution of the fluid in the channels at the center of the module. The fin temperature varies from 319 K to 322 K and the fluid temperature varies from 315 K to 319 K.

Reproduced with permission of the copyright owner. Further reproduction prohibited without permission.

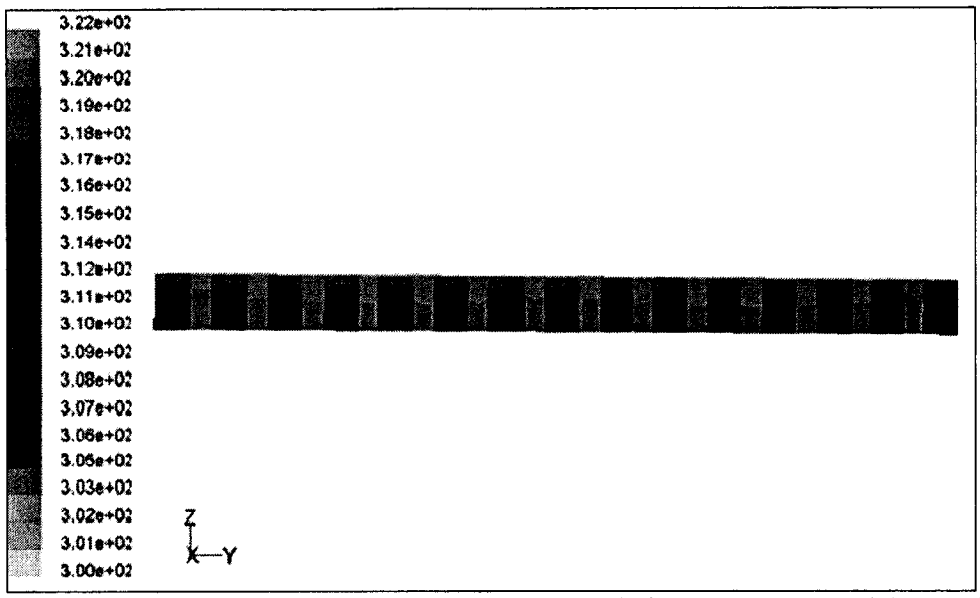

Figure 21 Temperature profiles [K] of the fin and fluid at the center of the module

Figure 22 shows the fluid temperature along the flow direction. The inlet fluid temperature is 315 K and at the outlet the temperature increased by 5 K to 320 K. It is almost a linear profile except for some spikes at the end. The temperature spike at the end the flow is caused by a stagnation of the flow at the exit of the module.

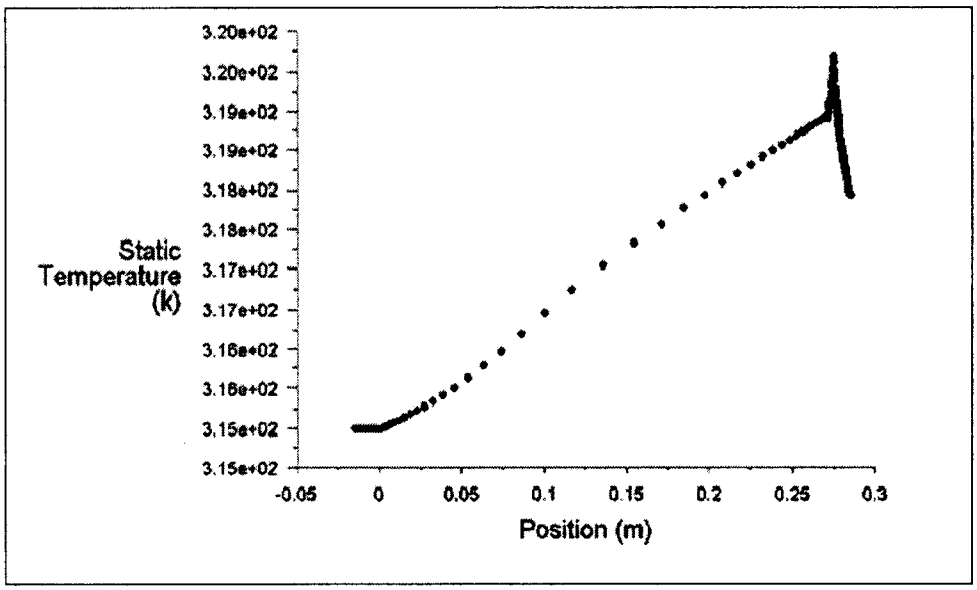

Figure 22 Fluid temperatures as function of position in the flow direction

Reproduced with permission of the copyright owner. Further reproduction prohibited without permission.

Figures 23 and 24 demonstrate the pressure drop in the channels for flow rates of 2.5 and 3.00 gpm per module. Mass flow rate and pressure drop are directly proportional to each other. As shown in those two figures, the pressure drop increases by 6300 Pa when the flow rate increased from 2.5 to 3 gpm per module.

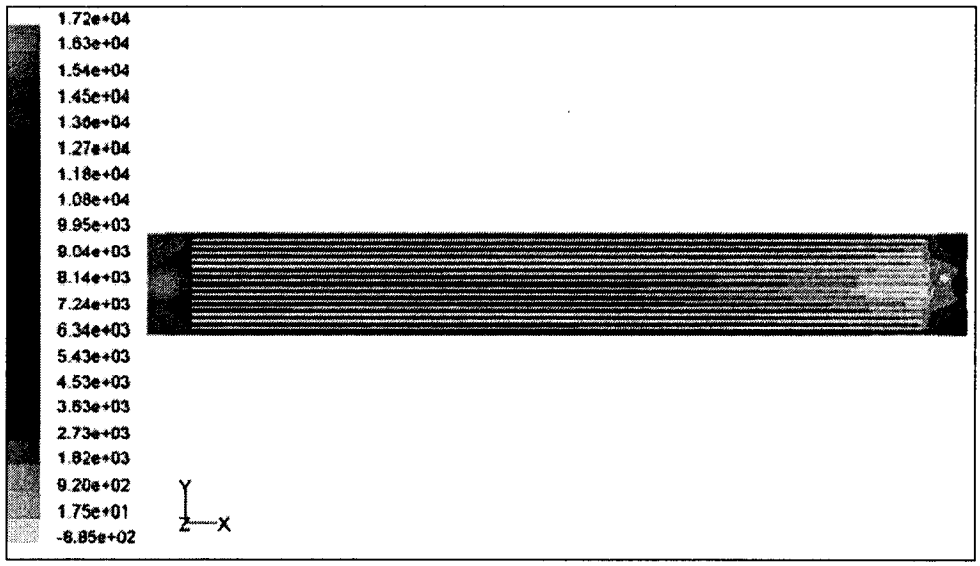

Figure 23 Contours of pressure drop [Pa] for flow rate of 2.5 gpm per module

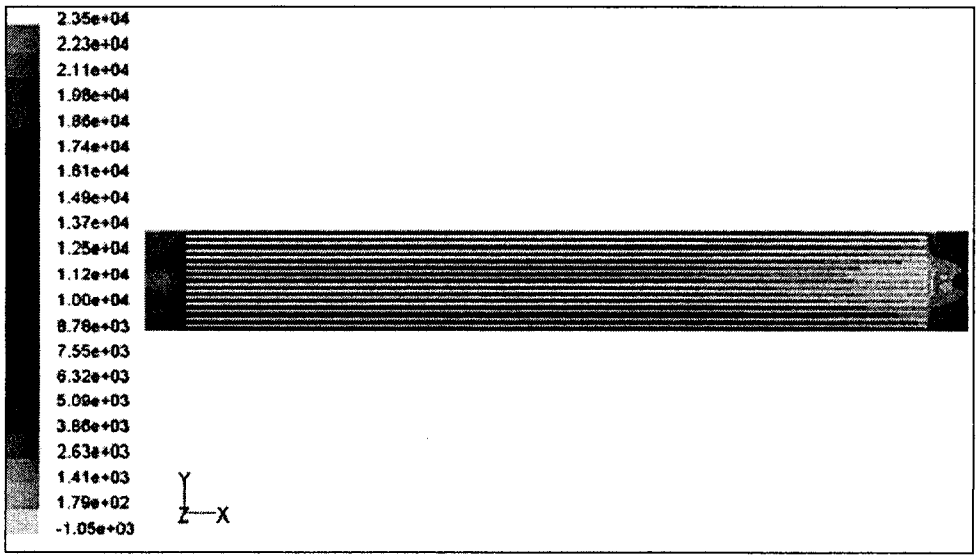

Figure 24 Contours of pressure drop [Pa] for flow rate of 3.00 gpm per module

Reproduced with permission of the copyright owner. Further reproduction prohibited without permission.

The maximum pressure is at the inlet of the module. Pressure drops of 17200 Pa and 23500 Pa are found for flow rates of 2.5 and 3.00 gpm respectively. The maximum pressure drop inside the channels varies from 9950 Pa for the flow rate of 2.5 gpm and 13700 Pa for flow rate of 3 gpm.

Reproduced with permission of the copyright owner. Further reproduction prohibited without permission.

CHAPTER 5

RESULTS AND DISCUSSION

Steady state, transient and CFD models have been presented. Fifteen and seventeen fin geometries show the desired average cell temperature. Results are summarized in tables below for both cases with their respective parameters.

Table 3 Summary of parameters and results for 15-fin geometry

15 Fin-geometry, Flow rate = 2.5 gpm per module	
Module Size	5.1 cm by 29 cm
Depth, y	3 mm
Width, w	2.1 mm
Thickness of fin, th	1 mm
Length, z	27 cm
Reynolds number, Re	13520
Convective coefficient, hfl	18058 W/m^2K
Heat flux, q``	250 kW/m^2
Inlet fluid temp., Tin	315 K
Cell temp., Tcell	62.8°C, 336 K
Pressure drop, ΔP	4454 Pa
Outlet fluid temp. Tout	318.5 K

Reproduced with permission of the copyright owner. Further reproduction prohibited without permission.

Table 4 Summary of parameters and results for 15-fin geometry

15 Fin-geometry, Flow rate = 3.00 gpm per module	
Module Size	5.1 cm by 29 cm
Depth, y	3 mm
Width, w	2.1 mm
Thickness of fin, th	1 mm
Length, z	27 cm
Reynolds number, Re	16400
Convective coefficient, hfl	21416 W/m^2K
Heat flux, q``	250 kW/m^2
Inlet fluid temp., Tin	315 K
Cell temp., Tcell	61.5°C, 334.6 K
Pressure drop, ΔP	5800 Pa
Outlet fluid temp. Tout	318 K

Table 5 Summary of parameters and results for 17-fin geometry

17 Fin-geometry, Flow rate = 2.5 gpm per module	
Module Size	5.1 cm by 29 cm
Depth, y	3 mm
Width, w	1.76 mm
Thickness of fin, th	1 mm
Length, z	27 cm
Reynolds number, Re	13021
Convective coefficient, hfl	19425 W/m^2K
Heat flux, q``	250 kW/m^2
Inlet fluid temp., Tin	315 K
Cell temp., Tcell	61.5°C, 334.65 K
Pressure drop, ΔP	5621 Pa
Outlet fluid temp. Tout	318.7 K

Reproduced with permission of the copyright owner. Further reproduction prohibited without permission.

Table 6 Summary of parameters and results for 17-fin geometry

17 Fin-geometry, Flow rate = 3.00 gpm per module	
Module Size	5.1 cm by 29 cm
Depth, y	3 mm
Width, w	1.76 mm
Thickness of fin, th	1 mm
Length, z	27 cm
Reynolds number, Re	15588
Convective coefficient, hfl	23008 W/m^2K
Heat flux, q``	250 kW/m^2
Inlet fluid temp., Tin	315 K
Cell temp., Tcell	60.4°C, 333.5 K
Pressure drop, ΔP	7200 Pa
Outlet fluid temp. Tout	317.7 K

These are the conditions under which the module is designed to operate and to give rated performance. The desired average operating cell temperature is 65°C. These two geometries are selected since they give the desired temperature, which is less than 65°C, and the pressure drop is in an acceptable range. The change in temperature at each surface is shown in Figure 25. The dielectric material has a low conductivity, and it is expected to experience higher temperature differences.

Reproduced with permission of the copyright owner. Further reproduction prohibited without permission.

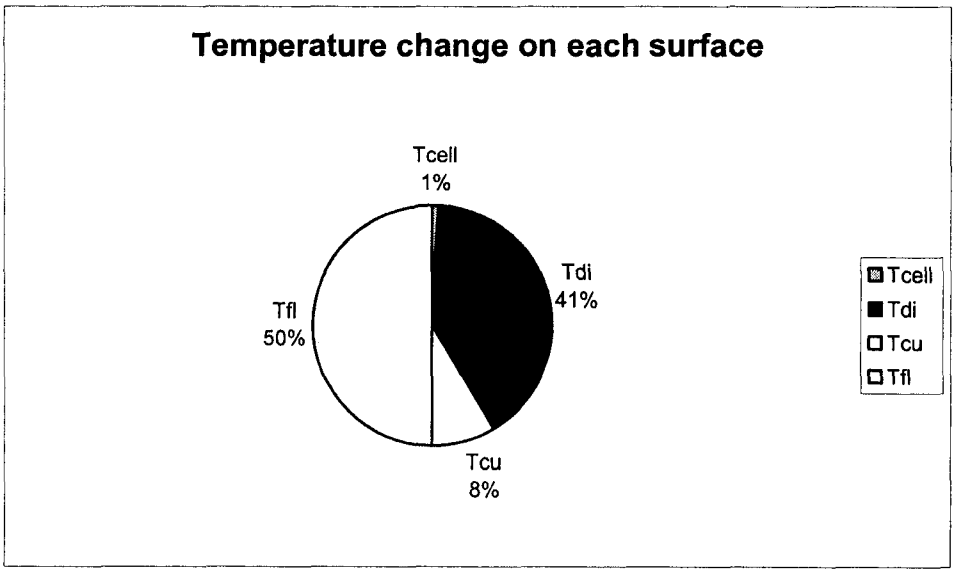

Figure 25 One-dimensional analysis of temperature change on each component

A dynamic model has been developed in order to simulate the cell temperature and efficiency. Two cases (time varying and constant solar flux) are presented and discussed. The equations described cell temperature as a function of time and length along the flow with reasonable precision. Although the total direct radiation absorbed by the solar cells as reflected by the mirror area, including transmissibility of the glass cover, absorptivity of the cells, scaling factors for reflectivity of the concentrator, the shading of the mirrors and the dirtiness of the mirrors, the analysis presented in this paper assumed the 1000 W/m^2 (250 suns) flux is directly absorbed by the cells. This assumption is reasonable for the maximum conditions in Las Vegas. During operation 15 to 20% of the total solar flux is converted to electrical output, which will result in the cell temperature being even lower. The analysis is performed based upon a zero electrical output. This will predict the maximum energy flow, which must be dissipated by the cooling system.

Reproduced with permission of the copyright owner. Further reproduction prohibited without permission.

The results shown in Figures 13 and 15 demonstrate the cell temperature behavior over time. The time required to reach the steady state in an instantaneously imposed heat flux is less than two seconds. Figure 13 shows the gradual increasing of temperature based on the flux. The model described the cells' temperature behavior based on the hourly input of solar flux. The flux goes down as the sun sets (around 27000 sec, 4:00PM) and that is shown in the analysis when the cell temperature starts to decrease after 4:00 PM. The time it took to reach a critical temperature without circulating cooling fluid is shown in Figure 16: less than a second and half to reach 400K.

The convection coefficient between the channel and the fluid changes significantly depending on whether or not the fluid flow in the passage is laminar or turbulent. Based on the passage size, geometry, viscosity and flow rate a turbulent flow (Re > 10000) is achieved. A convection correlation given by [4] is used to find a local Nusselt number for turbulent flow for rectangular geometry based on the hydraulic diameter. The correlation is valid for Reynold's number from 10000 to 10^6. The mass flow rate is reasonably constant for the application described in this paper, and therefore to simplify the calculation in this model, the convection coefficient is entered as a parameter in the model and assumed to be constant along the receiver. In Figure 26 the convective heat transfer coefficient increases almost linearly with the increase of number of channels. As the number of passages increased from five to twenty, the convective heat transfer coefficient increased by 8453 W/m^2K and the cell temperature decreased by 11 K. Figure 22 shows the cell temperature decreasing as the convective heat transfer increases. As it is observed in the analysis, the convective heat transfer coefficient is

Reproduced with permission of the copyright owner. Further reproduction prohibited without permission.

high. The system requires a high heat transfer coefficient in order to achieve lower cell temperatures.

A number of parameters affect the cell temperature in this investigation including: inlet fluid temperature, mass flow rate and thickness of the fins. Those parameters are evaluated for different ranges and plotted. The results demonstrate how the cell temperature behaves when one of the parameters changed. The results will be incorporated in the eventual optimization process.

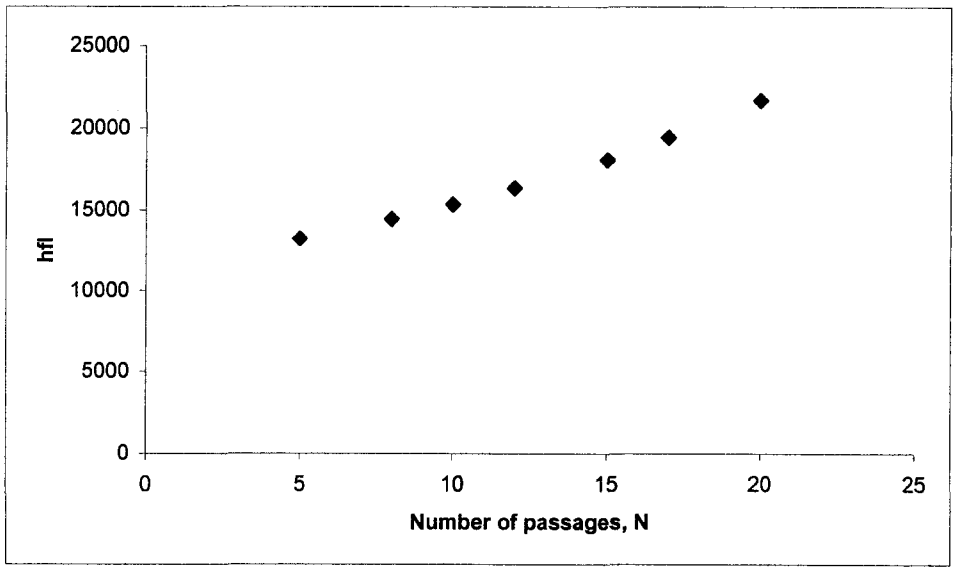

Figure 26 Number of passages versus convective heat transfer coefficient [$W/m^2 K$]

Reproduced with permission of the copyright owner. Further reproduction prohibited without permission.

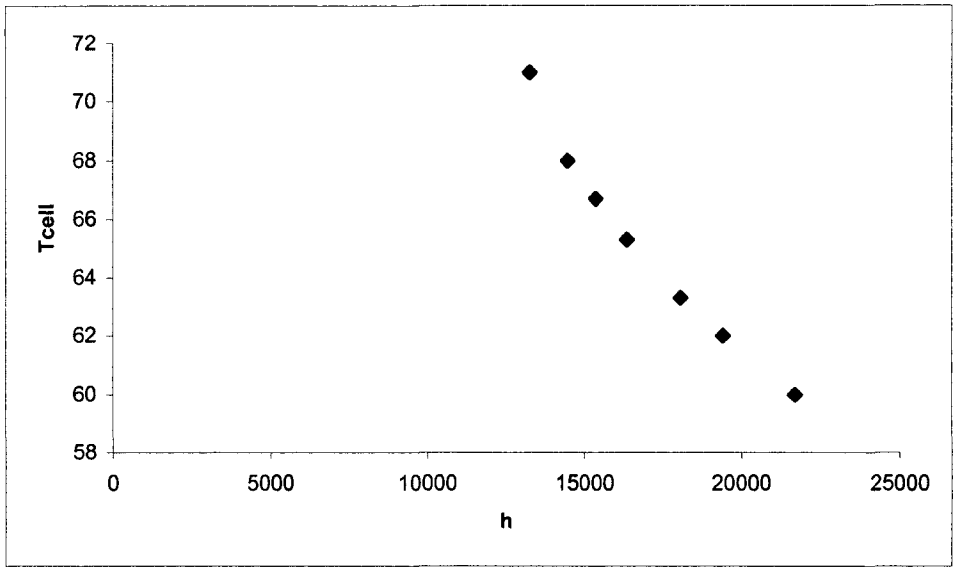

Figure 27 Convective heat transfer coefficient [$W/m^2 K$] versus cell temperature [$^{\circ}C$]

The inlet temperature is an important parameter. The average inlet fluid temperature is assumed to be entering the channels at 315 K (~42°C) based on the ambient temperature in the region. However, a study is done to observe the effect of inlet temperature by varying the inlet temperature from 300 K to 330 K (27 to 57°C) to observe a change in the cell temperature. The result shows a linearly increasing temperature as inlet temperature increases.

Reproduced with permission of the copyright owner. Further reproduction prohibited without permission.

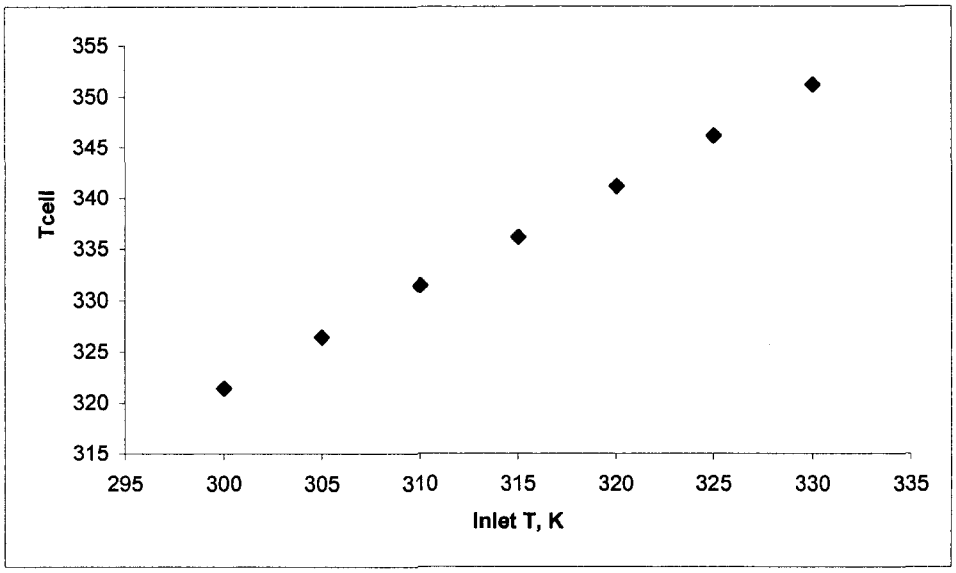

Figure 28 Inlet temperatures versus cell temperature [K]

Flow rate is another critical factor in this analysis. A flow of 0.1561 kg/sec per module (2.5 gpm) is used for the analysis in this paper considering the pump work required and the cell temperature. Figures 29 and 30 show the flow rate versus cell temperature and pressure drop respectively for the case of fifteen-fin geometry, 1 mm thick fin and inlet temperature of 315 K:

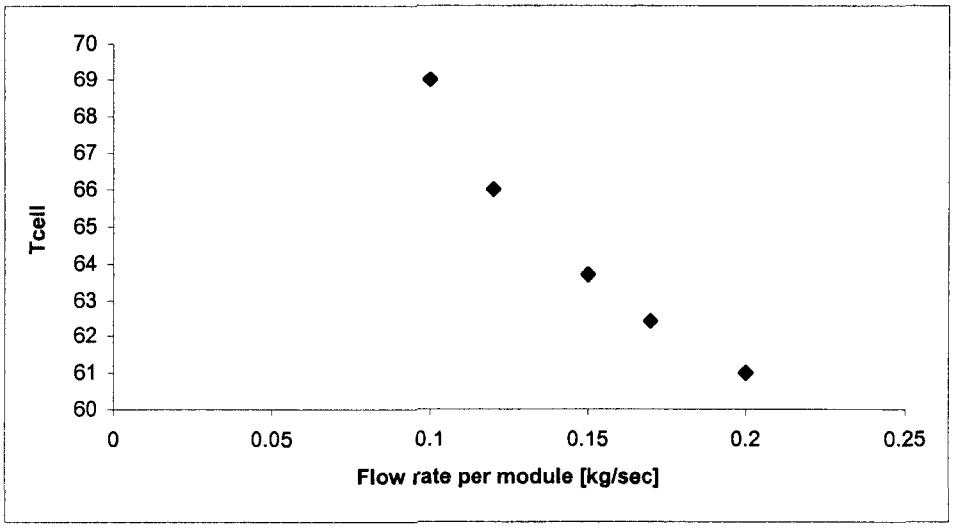

Figure 29 Flow rate [kg/sec] versus cell temperature [K]

Reproduced with permission of the copyright owner. Further reproduction prohibited without permission.

As it is shown in Figure 29, the cell temperature dropped from 69°C to 61°C when the flow rate increased from 0.1 kg/sec (1.58 gpm) to 1.9 kg/sec (3 gpm). However, the pressure drop increased by over 4000 Pa as seen in Figure 30.

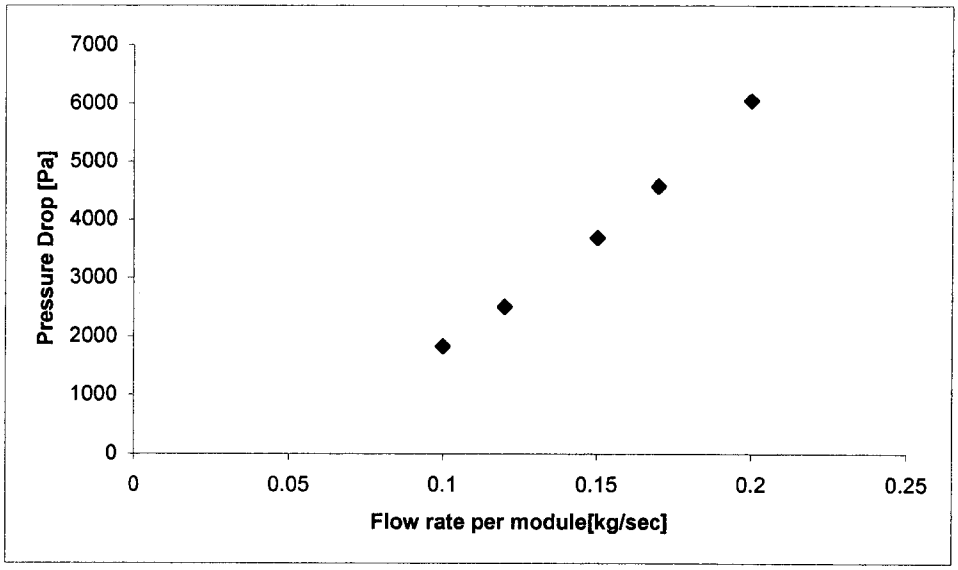

Figure 30 Flow rate [kg/sec] versus pressure drop [Pa]

The effect of fin thickness was also studied for the 15-fin geometry. The result shows as the fin thickness increases the cell temperature increases. When the fin thickness increases, the gap between the fins decreases and this causes a higher-pressure drop. Based machining capabilities and desired cell temperature 1 mm fin geometry is selected for this investigation.

Reproduced with permission of the copyright owner. Further reproduction prohibited without permission.

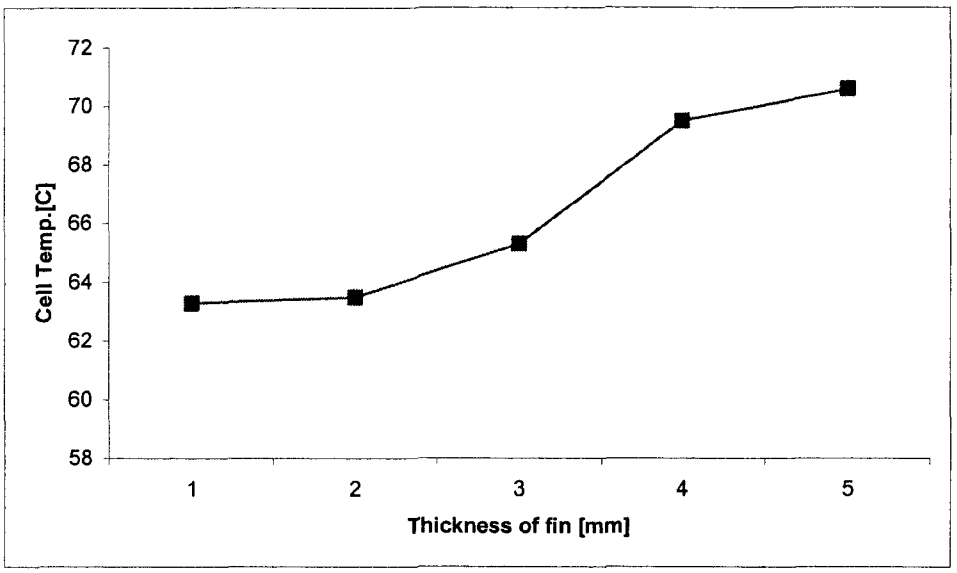

Figure 31 Thickness of fin [mm] versus cell temperature [°C]

Even though the length of the module (along the flow direction) is already specified, a study is made on the effect on cell temperature as well as the outlet fluid temperature. Figure 32 and 33 show a linear increase of cell temperature and outlet fluid temperature respectively as the channel length (z) increases from 5 to 55 cm.

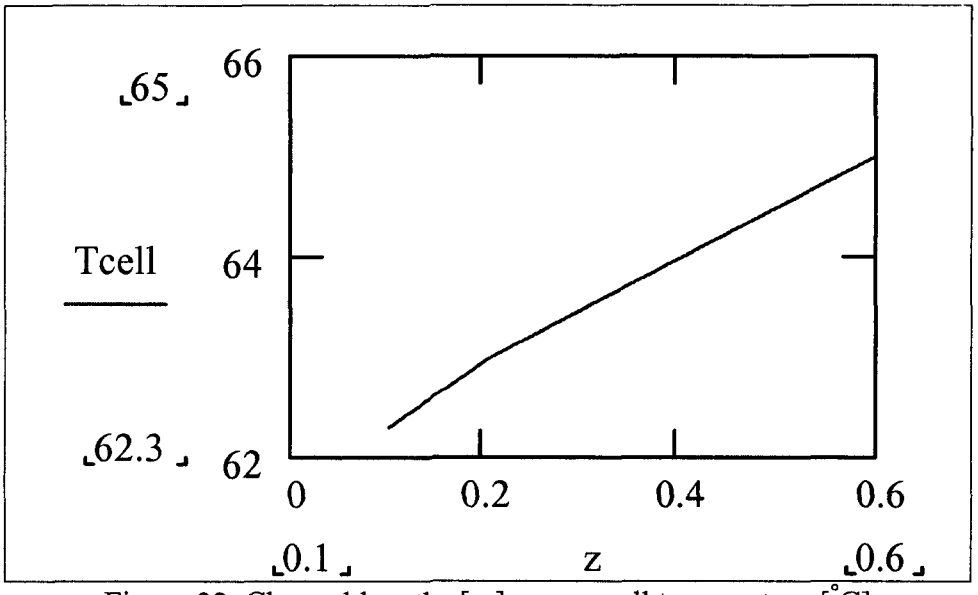

Figure 32 Channel lengths [m] versus cell temperature [°C]

Reproduced with permission of the copyright owner. Further reproduction prohibited without permission.

The cell and outlet temperatures increased by 3°C and 7°C respectively when the length of the module increased from 5 cm to 55 cm. The mass flow rate and the inlet fluid temperature are based on 2.5 gpm per module and 315 K respectively.

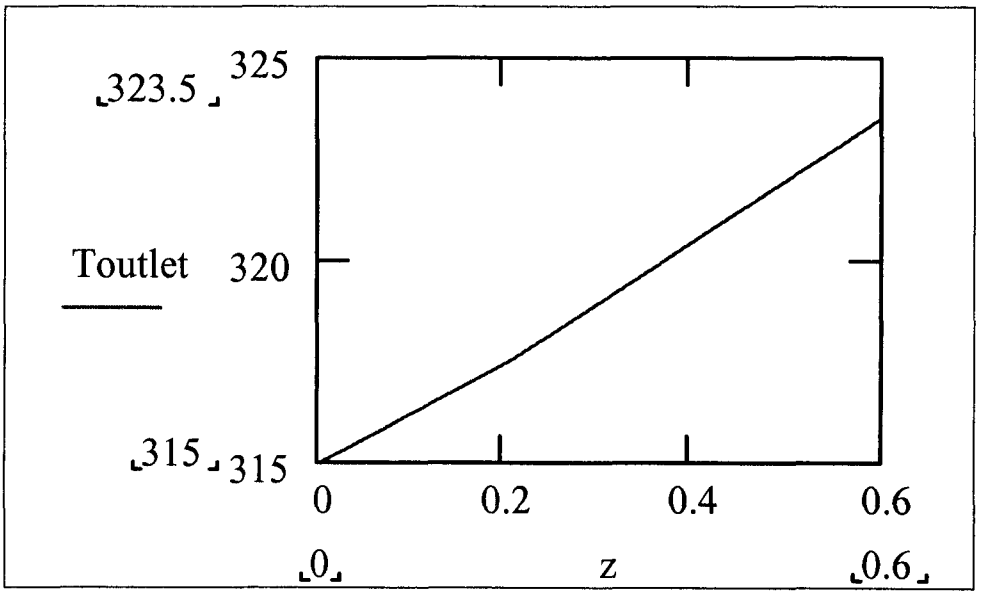

Figure 33 Channel lengths [m] versus outlet fluid temperature [K]

Computational validation is shown in Figures 19 to 22 for the cell temperature. The result shows the temperature distribution along and perpendicular to the flow. For the most part the wall temperature is in the range of the analytical result. Hotter wall temperatures are observed along the edges of the wall and at the exit of the flow. This is expected since the fluid heats up as it moves along. Increasing the flow rate can reduce this problem. However, the primary motivation of the system is to bring cost down and increasing flow rate requires higher pump work. This will require finding the optimum value that results in higher efficiency and lower cost. The cell efficiency of the conversion of solar insolation to DC power at peak power point under rated conditions is around 15%. See Table 7 for summary of analytical and CFD model results:

Reproduced with permission of the copyright owner. Further reproduction prohibited without permission.

Table 7 Summary of analytical and CFD models result

	Analytical Model	CFD Model
Mass flow rate	2.5 gpm/ module	2.5 gpm/ module
Number of channels	15	15
Inlet water temperature	315 K	315 K
Outlet water temperature	318.5 K	319
Average wall temperature	323 K	320 to 322 K
Average cell temperature	336 K	333 to 335 K
Pressure drop in the module		17200 Pa
Reynolds number	13520	14091
Heat transfer coefficient	18058 W/m^2 K	19343 W/m^2 K

Reproduced with permission of the copyright owner. Further reproduction prohibited without permission.

CHAPTER 6

PERFORMANCE OPTIMIZATION

The cooling system consisting of several automotive radiators, a fan, and a pumped liquid coolant loop has been analyzed independently. After both cases are investigated and analyzed separately, they are coupled and optimized. The MATLAB optimization toolbox is used to find the optimum performance of the whole system. Parameters: air flow rate, water flow rate, number of radiators, and number of channel per module are varied to achieve the optimum output for various ambient temperatures, pump and fan efficiencies. Based on the developed analysis, performance of the system as a function of system design parameters is shown:

$$\text{System\_Efficiency} = \frac{\text{Electric\_power} - \text{Fan\_power} - \text{Pump\_power}}{[(\text{Total\_Solar\_Flux}) \cdot \text{Area\_module}]}$$

Reproduced with permission of the copyright owner. Further reproduction prohibited without permission.

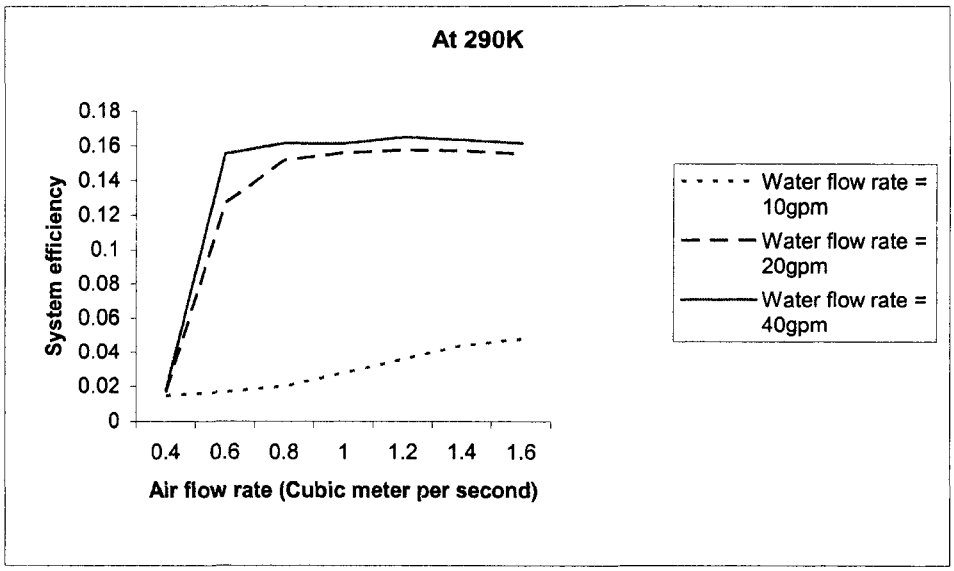

Figure 34 System efficiency as functions of ambient temp., liquid, and air flow rate

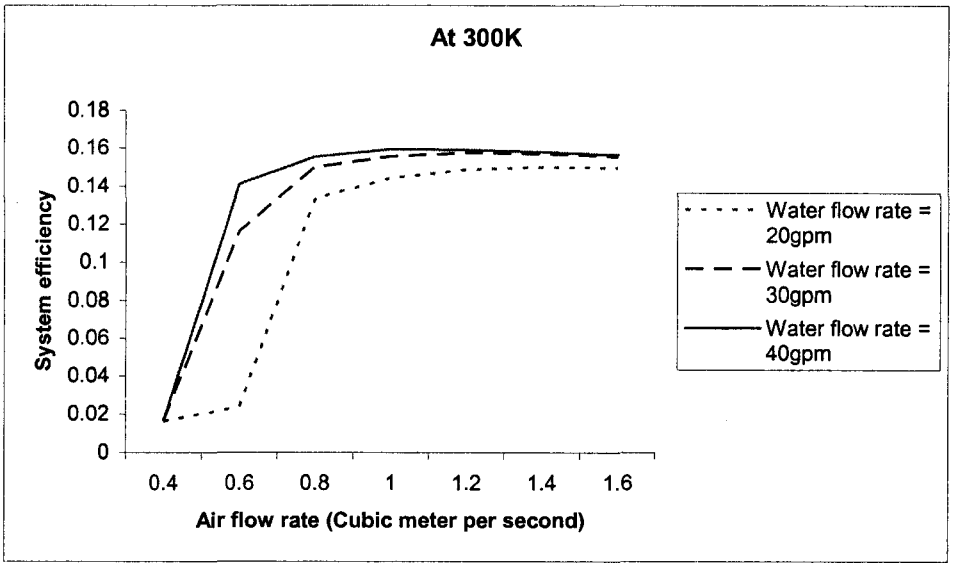

Figure 35 System efficiency as functions of ambient temp., liquid, and air flow rate

Reproduced with permission of the copyright owner. Further reproduction prohibited without permission.

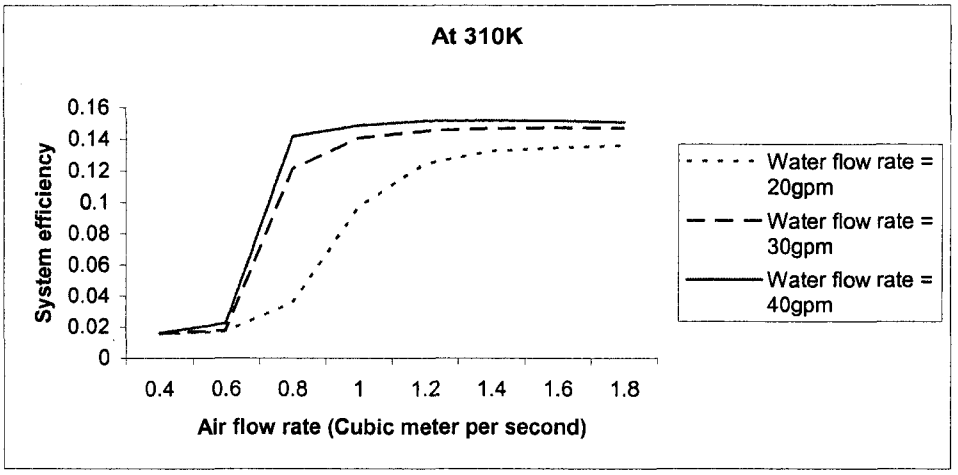

Figure 36 System efficiency as functions of ambient temp., liquid, and air flow rate

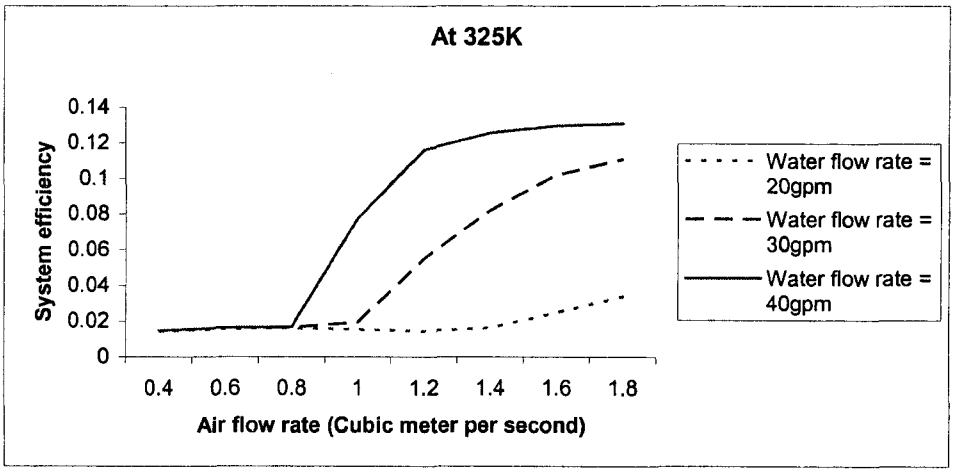

Figure 37 System efficiency as functions of ambient temp., liquid, and air flow rate

The following conditions are under which the module is desired to operate and give rated performance:

Table 8 The overall optimized system efficiency and input parameters

# Radiator	# Channels	Water flow rate gpm	Air flow rate m^3/sec	Max. Electric output kW	Ave. Electric output kW	Ave. System efficiency. %	Max. System efficiency %	Max. Tamb K	Min. Tamb K
4	15	40	1.5	13.7	12.5	14.9	16.15	325	290

Reproduced with permission of the copyright owner. Further reproduction prohibited without permission.

CHAPTER 7

CONCLUSIONS

The steady state model predicted temperature at each surface of the unit. Based on the temperature distribution, different parameters were changed to get the desired operating cell temperature. Most of the heat has to be rejected to the circulating fluid. The forced convection heat transfer coefficient term has to be very high in order to have lower cell temperatures. Lower hydraulic diameter increased the heat transfer coefficient term but it also increases the pressure drop in the passages. This is shown in detail in the model.

The transient model reveals the time elapsed for the cells to reach a steady state and critical temperature. The transient analysis predicted that it would take a very short period of time for the cells to reach a higher temperature. This will require a fast shutting system to avoid damaging cells from high solar flux when a malfunction happens during operation.

The developed models predict cell temperature. Based on the predicted cell temperatures the efficiency of the cells is determined. A good agreement between the analytical and the computational model is observed. The model gave the desired operating cell temperature.

Optimization of the whole system is finalized. The mass flow rate, size of channel, pump work and cell temperature parameters are varied to achieve the optimum output.

Reproduced with permission of the copyright owner. Further reproduction prohibited without permission.

Based on the developed analysis, performance of the system as a function of system design parameters is shown.

Reproduced with permission of the copyright owner. Further reproduction prohibited without permission.

APPENDIX A

NOMENCLATURE

A	surface area of aperture (m^2)
c	specific heat (J/kg K)
h	convection coefficient (W/m^2 K)
L	depth of the passage (m)
m	flow rate of fluid (kg/sec)
q``	solar flux (W/m^2)
s	Laplace transform
T	temperature (K, $^{\circ}C$)
t	time (sec)
th	thickness (m)
V	volume of the channel (m^3)
w	width of the passage (m)
y	depth of the passage from L=0 to L (m)
z	length of the passage (m)
ρ	density of fluid (kg/m^3)
κ	conductivity (W/m K)

Subscript

di	dielectric material
cu	top surface of copper plate (wall)
fl	fluid or coolant
in	inlet
out	outlet
ribs	fins
cell	solar cell
z, t	partial with respect to

Reproduced with permission of the copyright owner. Further reproduction prohibited without permission.

APPENDIX B

MATHCAD AND MATLAB PROGRAMS

Mathcad and MATLAB programs are used to evaluate the steady state and transient models. The five ordinary differential equations are solved using Laplace transform using Mathcad's symbolic tool bar. The optimization of the whole system is done using the MATLAB optimization toolbox.

Mathcad Program

$$qs \cdot w \cdot z - \frac{\kappa cell \cdot (Tcell - Tsi)}{thcell} \cdot w \cdot z = 0$$

$$qs \cdot w \cdot z - \frac{\kappa cell}{thcell} \cdot w \cdot z \cdot Tcell + \frac{\kappa cell}{thcell} \cdot w \cdot z \cdot Tsi = 0$$

$$\frac{\kappa cell \cdot (Tcell - Tsi)}{thcell} \cdot w \cdot z - \frac{\kappa si \cdot (Tsi - Tcu)}{thsi} \cdot w \cdot z = 0$$

$$\left(\frac{-\kappa cell}{thcell} \cdot w \cdot z - \frac{\kappa si}{thsi} \cdot w \cdot z \right) \cdot Tsi + \frac{\kappa cell}{thcell} \cdot w \cdot z \cdot Tcell + \frac{\kappa si}{thsi} \cdot w \cdot z \cdot Tcu = 0$$

$$\frac{\kappa si \cdot (Tsi - Tcu)}{thsi} \cdot w \cdot z - hfl \cdot (w) \cdot z \cdot (Tcu - Twat) - \frac{\kappa cu \cdot (Tcu - Tbase) \cdot 2 \cdot thfin \cdot z}{L} = 0$$

$$(-2 \cdot hfl \cdot z \cdot thfin + hfl \cdot z \cdot w) \cdot Twat + \left(-hfl \cdot z \cdot w + 2 \cdot hfl \cdot z \cdot thfin - \frac{\kappa si}{thsi} \cdot w \cdot z - 2 \cdot \kappa cu \cdot thfin \cdot \frac{z}{L} \right) \cdot Tcu +$$

$$\frac{\kappa si}{thsi} \cdot w \cdot z \cdot Tsi + 2 \cdot \kappa cu \cdot thfin \cdot \frac{z}{L} \cdot Tbase = 0$$

Reproduced with permission of the copyright owner. Further reproduction prohibited without permission.

$$\frac{\kappa cu\cdot(Tcu - Tbase)\cdot 2\cdot thfin\cdot z}{L} - hfl\cdot z\cdot\left[\int_0^L \left[\left[(Tbase - Tcu)\cdot\frac{y}{L} + Tcu\right] - Twat\right] dy\right] = 0$$

$$\left(2\cdot\kappa cu\cdot thfin\cdot\frac{z}{L} - \frac{1}{2}\cdot hfl\cdot z\cdot L\right)\cdot Tcu + \left(-2\cdot\kappa cu\cdot thfin\cdot\frac{z}{L} - \frac{1}{2}\cdot hfl\cdot z\cdot L\right)\cdot Tbase + hfl\cdot z\cdot Twat\cdot L = 0$$

$$[mdot\cdot Cfl\cdot[Tin - (2\cdot Twat - Tin)] + hfl\cdot(w - 2\cdot thfin)\cdot z\cdot(Tcu - Twat)]$$

$$hfl\cdot z\cdot\left[\int_0^L \left[\left[(Tbase - Tcu)\cdot\frac{y}{L} + Tcu\right] - Twat\right] dy\right] = 0$$

$y := .003$ $L1 := .003$ $\kappa fl := 0.55$ $w := 0.00213$ $mdot := 0.01262$ $Cfl := 3800$

$\rho := 1050$ $Tamb := 315$ $C_{cu} := 385$ $qs := 250000$

$D_h := \frac{4\cdot y\cdot w}{2\cdot(y + w)}$ $D_h = 2.491 \times 10^{-3}$ $Tin := 315$ $z := 0.27$

$Pr := 3.77$ $\mu f := .3\cdot 10^{-3}$ $\mu 1w := 240\cdot 10^{-6}$

$Re := \frac{mdot\cdot D_h}{y\cdot w\cdot\mu f}$ Re = function

$f := (0.79\cdot\ln(Re) - 1.64)^{-2}$ $f = 0.028$ $Nu := \frac{\frac{f}{8}\cdot(Re - 1000)\cdot Pr}{1 + 12.7\cdot\left(\frac{f}{8}\right)^{0.5}\cdot\left(Pr^{\frac{2}{3}} - 1\right)}$

$hfl := \frac{Nu\cdot\kappa fl}{D_h}$ $hfl = 2.142 \times 10^4$ $Nu = 97.005$

$thcell := 1\cdot 10^{-4}$ $\kappa cell := 138$ $thsi := 8\cdot 10^{-5}$ $\kappa si := 2.2$ $thfin := 0.001$ $\kappa cu := 401$

$$qs\cdot w\cdot z - \frac{\kappa cell}{thcell}\cdot w\cdot z\cdot Tcell + \frac{\kappa cell}{thcell}\cdot w\cdot z\cdot Tsi = 0 \qquad \text{---------eq1}$$

Reproduced with permission of the copyright owner. Further reproduction prohibited without permission.

$$qs \cdot w \cdot z - \frac{\kappa cell}{thcell} \cdot w \cdot z \cdot Tcell + \frac{\kappa cell}{thcell} \cdot w \cdot z \cdot Tsi = 0 \qquad \text{--------eq1}$$

$$\left(\frac{-\kappa cell}{thcell} \cdot w \cdot z - \frac{\kappa si}{thsi} \cdot w \cdot z\right) \cdot Tsi + \frac{\kappa cell}{thcell} \cdot w \cdot z \cdot Tcell + \frac{\kappa si}{thsi} \cdot w \cdot z \cdot Tcu = 0 \qquad \text{--------eq2}$$

$$(-2 \cdot hfl \cdot z \cdot thfin + hfl \cdot z \cdot w) \cdot Twat + \left(-hfl \cdot z \cdot w + 2 \cdot hfl \cdot z \cdot thfin - \frac{\kappa si}{thsi} \cdot w \cdot z - 2 \cdot \kappa cu \cdot thfin \cdot \frac{z}{L}\right) \cdot Tcu$$

$$\frac{\kappa si}{thsi} \cdot w \cdot z \cdot Tsi + 2 \cdot \kappa cu \cdot thfin \cdot \frac{z}{L} \cdot Tbase = 0 \qquad \text{----eq3}$$

$$\left(2 \cdot \kappa cu \cdot thfin \cdot \frac{z}{L} - \frac{1}{2} \cdot hfl \cdot z \cdot L\right) \cdot Tcu + \left(-2 \cdot \kappa cu \cdot thfin \cdot \frac{z}{L} - \frac{1}{2} \cdot hfl \cdot z \cdot L\right) \cdot Tbase + hfl \cdot z \cdot L \cdot Twat = 0 \qquad \text{----eq4}$$

$$(-2 \cdot mdot \cdot Cfl - hfl \cdot z \cdot w - hfl \cdot z \cdot L + 2 \cdot hfl \cdot z \cdot thfin) \cdot Twat + \left(hfl \cdot z \cdot w + \frac{1}{2} \cdot hfl \cdot z \cdot L - 2 \cdot hfl \cdot z \cdot thfin\right) \cdot Tcu +$$

$$2 \cdot mdot \cdot Cfl \cdot Tin + \frac{1}{2} \cdot hfl \cdot z \cdot L \cdot Tbase = 0 \qquad \text{-----eq5}$$

MATLAB Program

```
function module=f(Q_L,TL_in,mix,qsol,nc)

% This function takes the following arguments
%Q_L=Volume flow rate of liquid (m^3/s)
%TL_in=Cell inlet water temp K
%mix=volume fraction of coolant if aqueous solution is used
%qsol=direct normal solar flux W/m^2 at receiver
%nc=# channels per module
%It outputs
%cell temp K
%electrical output W
%outlet temp (K)
% Cell module geometry
Cd=3/1000;  % Channel depth (m)
ft=1/1000;  % Fin thickness of inner fins(m)
fto=2/1000;  % Fin thickness of outer fins(m)
wm=5/100;   %module width (m)
Lm=54/100;   % length of 2 modules (m)
wc=(wm-2*fto-(nc-1)*ft)/nc; %Channel width
Dhc=(4*Cd*wc)/(2*(Cd+wc)); % hydraulic diameter
nm=12; %#modules
td=.00008; %Thickness of dielectric  (m)
```


Reproduced with permission of the copyright owner. Further reproduction prohibited without permission.

```
kd=2.2; %Thermal conductivity of dielectric (W/mK)
tcop=(1/8)*(2.54/100);%Thickness of copper (m)
kcop=401; %Thermal conductivity of copper
r=wc/Cd; %ratio of channel width and depth

CellEff=[.2448 .223 .2064 .2016 .1937 .1920 .1776 .1749 .1642 .1550 .147 .14 .125 .111
.085 .063 .036 .021 0];

TCellEff=[ 8.6 11.6 17.2 22.6 34.5 50.3 58.4 68.5 76.5 82.3 85 87 90 92 95 97 99 100
300]+273.15;

delta_x=.5*2.54/100;
n=1;
TL=TL_in;
Tdi_out=TL_in+10;
eff=interp1(TCellEff,CellEff,Tdi_out);
q=(qsol-eff*qsol)*((wc+ft)*delta_x);

while n*delta_x<=Lm

  Re=((DensMix(TL,mix))*Dhc*(Q_L/(nm*nc*wc*Cd)))/VisMix(TL,mix);
  Pr=VisMix(TL,mix)*Cpmix(TL,mix)/CondMix(TL,mix);
  if Re<=2300
    if r <=1
      F=57/Re;
      Nu=3.61;

    elseif 1<r<=1.43
      F=59/Re;
      Nu=3.73;
    elseif 1.43<r<=2
      F=62/Re;
      Nu=4.12;
    elseif 2<r<=3
      F=69/Re;
      Nu=4.79;
    elseif 3<r<=4
      F=73/Re;
      Nu=5.33;
    elseif r>4
      F=82/Re;
      Nu=6.49;

    end

  else
```


Reproduced with permission of the copyright owner. Further reproduction prohibited without permission.

```
    F=.316*(Re^(-.25));
    Nu=((F/8)*(Re-1000)*Pr)/(1+(12.7*(F/8)^.5)*((Pr^.667)-1));
  end

  cf=F/4;
  h=Nu*(CondMix(TL,mix))/Dhc;
  Tc=(q+(h*wc*delta_x*TL)+(h*Cd*delta_x*TL))/(h*delta_x*(wc+Cd));
  mdot=(Q_L/(nm*nc))*DensMix(TL,mix);
  TL=TL+(q/(mdot*Cpmix(TL,mix)));
  Tliquid(n)=TL;
  Tcopper_in(n)=Tc;
  Tcopper_out(n)=(q*tcop/(kcop*wc*delta_x))+Tcopper_in(n);
  Tdi_out(n)=(q*td/(kd*wc*delta_x))+Tcopper_out(n)-10;

    eff(n)=interp1(TCellEff,CellEff,Tdi_out(n));

  q=(qsol-eff(n)*qsol)*((wc+ft)*delta_x);
  El(n)=qsol*eff(n)*((wc+ft)*delta_x);
  V=Q_L/(nm*nc*wc*Cd);
  delta_P(n)=(DensMix(TL,mix)*(V^2)*cf*(delta_x*2*(Cd+wc)))/(2*Cd*wc);
  n=n+1;
end

eff;
delta_P;
edot=nc*nm*sum(El);
delta_P_total=sum(delta_P);
Tliquid;
Tcopper_in;
Tcopper_out;
Tdi_out;
Tcell=Tdi_out;
Re;
Wp=Q_L*delta_P_total;
q_in=qsol*Lm*wm*nm;

module=[delta_P_total,Wp,edot,Tliquid(n-1),Tcell(n-1),q_in];
function rad_SI=f(Q_A_std,QL,mix,Tamb,TL_in,nr)
%This function uses empirical data to predict the outlet liquid temperature
%for the radiators used in this project.
%It takes as arguments
%Q_A=volume flow rate of air (m^3/s) std
%Q_L=volume flow rate of liquid (m^3/s)
%mix=volume fraction of glycol
%Tamb=Ambient air temp (K)
%TL_in=Inlet liquid temp (K)
```


Reproduced with permission of the copyright owner. Further reproduction prohibited without permission.

```
%nr=number of radiators

%Radiator geometry

L=24.5*2.54/100;  %Core Length in meters
W=26.5*2.54/100;  %Core Width in meters
d=2*2.54/100;     %Core depth in meters
N=55; %number of tube banks
At=.00002196; %Tube cross sectional area (m^2)
Aw=.016; %Tube wall area (m^2)
pt=.026; % The tube perimeter is (m)
Dh=.003372; %The tube hydraulic diameter is (m)
Aff=.334; %free flow area of the air side of the core (m^2)
Lf=(3/8)*2.54/100;    %Fin length (m)
Fp=472.4; %number of fins per meter
%Empirical relation for liquid side
ReL_em=1000*[0  0.0774  0.1736  0.3054  0.4197  0.4959  0.6004  0.8993
1.4175];
NuL_em=[0  7.2085  7.3008  13.6705  14.1779  14.0856  15.9166  17.8016
19.3592];
%Empircal relation for air side
Nua_em=1000*[0  0.23811  0.42930  0.62400  0.77014 0.95720  1.11964];
Rea_em=10000*[0  0.16816  0.46270  0.67163  1.00442 1.49878  1.69634];

Tbulk_a_diff=2;
Tbulk_a=Tamb;

Tbulk_L_diff=2;
Tbulk_L=TL_in;
Q_A=Q_A_std/nr;
Q_L=QL/nr;

while abs(Tbulk_L_diff)>=1 | abs(Tbulk_a_diff)>=1

  ReL=(DensMix(Tbulk_L,mix)*Dh)*(Q_L)/(VisMix(Tbulk_L,mix)*At*3*N);
  if ReL >= ReL_em(9)
    NuL=2*10^-8*ReL^3-5*10^-5*ReL^2+.0494*ReL+1.4125;
  else
    NuL=interp1(ReL_em,NuL_em,ReL);
  end

  Rea=(DenseAir(Tbulk_a)*(Q_A/Aff)*d)/VisAir(Tbulk_a);
  Nua=interp1(Rea_em,Nua_em,Rea);
  ha_a=(Nua/d)*CondAir(Tbulk_a)*N*Fp*L*Lf*d;
  ha_L=(NuL/Dh)*CondMix(Tbulk_L,mix)*N*L*3*pt;
  UA_inv=(1/ha_a)+(1/ha_L);
```


Reproduced with permission of the copyright owner. Further reproduction prohibited without permission.

```
   UA=1/UA_inv;
   Ch=Cpmix(Tbulk_L,mix)*DensMix(Tbulk_L,mix)*(Q_L);
   Cc=CpAir(Tbulk_a)*DenseAir(Tbulk_a)*(Q_A);
   if Ch >= Cc
      Cmax=Ch;
      Cmin=Cc;
   end
   if Cc > Ch
      Cmax=Cc;
      Cmin=Ch;
   end
   NTU=UA/Cmin;
   Cr=Cmin/Cmax;
   VAR1=exp(-Cr*NTU^.78)-1;
   VAR2=(1/Cr)*NTU^.22;
   Eff=1-exp(VAR1*VAR2);
   TL_out=(Eff*Cmin*(TL_in-Tamb)-(Ch*TL_in))/(-Ch);
   qdot=Eff*Cmin*(TL_in-Tamb);
   Ta_out=((Eff*Cmin*(TL_in-Tamb))+Cc*Tamb)/Cc;
   Tbulk_a_new=(Tamb+Ta_out)/2;
   Tbulk_a_diff=(Tbulk_a-Tbulk_a_new);
   Tbulk_a=Tbulk_a_new;
   Tbulk_L_new=(TL_in+TL_out)/2;
   Tbulk_L_diff=(Tbulk_L-Tbulk_L_new);
   Tbulk_L=Tbulk_L_new;
   Q_A=Q_A_std*(Tbulk_a/293.15);
end

qdot_total=qdot*nr;

%Empirical relation for radiator air side (frictional)

CFA=[ 0.831 0.780 0.580 0.491 0.423 0.393 0.360 0.332 0.320 0.283 0.279 0.280 0.284
0.272 0.262 0.255 0.241 0.236 0.228 0.219 0.213 0.207 0.201 0.195 0.190 0.191 0.186
0.185 0.183 0.179 0.178 0.176 0.174 0.171];
RE_CFA=[ 1.399e3 1.667e3 2.161e3 2.779e3 3.519e3 4.012e3 4.751e3 5.267e3 5.917e3
6.970e3 7.463e3 7.822e3 8.517e3 9.144e3 1.013e4 1.080e4 1.161e4 1.255e4 1.340e4
1.434e4 1.520e4 1.596e4 1.694e4 1.784e4 1.838e4 1.865e4 1.910e4 1.954e4 2.004e4
2.057e4 2.089e4 2.125e4 2.205e4 2.286e4];

Kav=37.02;
Cfl=Kav/ReL;
Cfa=interp1(RE_CFA,CFA,Rea);
delta_P_L=Aw*(DensMix(Tbulk_L,mix))*Cfl*((Q_L/(At*3*N))^2)/(2*At);
delta_P_a=(d*Lf*Fp*L*N*(DenseAir(Tbulk_a))*Cfa*((Q_A/Aff)^2))/(2*Aff);
Wp=Q_L*nr*delta_P_L;
```


Reproduced with permission of the copyright owner. Further reproduction prohibited without permission.

```
Wf=Q_A*nr*delta_P_a;
rad_SI=[Tbulk_L,Tbulk_a,delta_P_L,delta_P_a,Wp,Wf];

function PV=f(Z)

%This function determines the steady state efficiency of the entire system
%It takes as arguments
%Q_A=volume flow rate of air (m^3/s) std
%Q_L=volume flow rate of liquid (m^3/s)
%nr=number of radiators in paralell
%nc=# channels per module

q_norm=1000;
mix=0;
Tamb=325;
eta_f=.8;
eta_p=.7;

Q_A_std=Z(1);
Q_L=Z(2);
nr=Z(3);
nc=Z(4);

CR=250; %concentration ratio of collector
qsol=CR*q_norm;
TL_in_guess=315; %TL_in_guess=Initial guess for inlet liquid temp to module (K)
TL_in_diff=10;
TL_in=TL_in_guess;
while TL_in_diff >=.5
   X=module(Q_L,TL_in,mix,qsol,nc);
   TL_out=X(4);
   Y=rad_SI(Q_A_std,Q_L,mix,Tamb,TL_out,nr);
   TL_in_diff=abs(TL_in-Y(1));
   TL_in=Y(1);
end

Wp=((X(2)+Y(5))/eta_p);
Wf=Y(6)/eta_f;
El=X(3);
qin=X(6);
T_cell_max=X(5);
q_net=El-Wp-Wf;
Eff_sys=q_net/qin;
delta_P_L=X(1)+Y(3);
delta_P_A=Y(4);
PV=[El,Wp,Wf,Eff_sys,T_cell_max,delta_P_L,delta_P_A];
```


Reproduced with permission of the copyright owner. Further reproduction prohibited without permission.

```
clear; clc

%     [Q_A,Q_L,nr,nc]

lb = [1.8,.00254,4,15];       % Set lower bounds
ub = [1.8,.00254,4,15];       % Set upper bounds

Zguess=[(lb(1)+ub(1))/2,(lb(2)+ub(2))/2,(lb(3)+ub(3))/2,(lb(4)+ub(4))/2];

options = optimset('LargeScale','off','Display','iter','MaxFunEvals',1000,'TolFun',.001);
[Z]= fmincon(@Eff_inv,Zguess,[],[],[],[],lb,ub,[],options);

Z;

M=[Z(1),Z(2),round(Z(3)),round(Z(4))];

B=PV(Z);

disp(['Volume flow rate of air (m^3/s) = ', num2str(M(1))]);
disp(['Volume flow rate of liquid (m^3/s) = ', num2str(M(2))]);
disp(['Number of radiators = ', num2str(M(3))]);
disp(['Number of channels per module = ', num2str(M(4))]);
disp(['Electrical output (W) = ', num2str(B(1))]);
disp(['Pump power (W) = ', num2str(B(2))]);
disp(['Fan power (W) = ', num2str(B(3))]);
disp(['System efficiency % = ', num2str(B(4)*100)]);
disp(['Max cell temperature (K)  = ', num2str(B(5))]);
disp(['Air side pressure drop (Pa)  = ', num2str(B(7))]);
disp(['Liquid side pressure drop (Pa)  = ', num2str(B(6))]);
```


Reproduced with permission of the copyright owner. Further reproduction prohibited without permission.

APPENDIX C

COMPUTATIONAL FLUID DYNAMICS FLOW MODELING

Preprocessing is the first step in building and analyzing a flow model. It includes building the model (or importing from a CAD package), applying a mesh, and entering the data. GAMBIT is one of the preprocessing tools. GAMBIT can import geometry from virtually any CAD/CAE software in Parasolid, ACIS, STEP or IGES format. Different CFD problems require different mesh types, and GAMBIT provides most of the options. The meshing toolkit lets you decompose geometries for structured hex meshing or perform automated hex meshing with control over clustering. Triangular surface meshes and tetrahedral volume meshes can be created within a single environment, along with Cartesian core, pyramids and prisms for hybrid meshing using automatic size distribution to correctly capture sharp curvature and small gaps. After preprocessing, the CFD solver does the calculations and produces the results. One of the most widely used CFD solvers is FLUENT. It is a finite volume based solver. General modeling capabilities include: complete mesh flexibility, all speed regimes (low subsonic, transonic, supersonic, and hypersonic flows), steady state, transient flows, inviscid, laminar, turbulent flows, Newtonian or non-Newtonian flows, Full range of turbulence models from simple k-epsilon models to large eddy simulation (LES), and Heat transfer including forced, natural, and mixed convection, conjugate heat transfer, as well as several radiation models.

Reproduced with permission of the copyright owner. Further reproduction prohibited without permission.

REFERENCES

[1] Science Applications International Corporation (SAIC), Specifications for a PV Receiver and Inverter System for the SAIC Dish Concentrator, UNLV Subcontract #03-SAIC-00.

[2] S. Yoon, Reduced Temperature Dependence of High Concentration PV Cell, Proc. IEEE Photovoltaic, 1994, pp. 1500-1504.

[3] AMONIX NREL Phase One Test Results for SAIC Dish Concentrator 030703.

[4] Incropera, Frank P., and Dewitt, 1996, Introduction to Heat Transfer, 3rd edition, John Wiley & Sons, New York.

[5] Myers, Glen E., 1998, Analytical Methods Conduction Heat Transfer, 2nd edition, AMCHT Publication, Madison, WI.

[6] Duffie, J.A., and Beckman, W.A., 1991, Solar Engineering of Thermal Processes, 2nd edition, John Wiley and Sons, New York.

[7] Kays, W.M., and Crawford, M.E., 1993, Convective Heat and Mass Transfer, 3rd edition, McGraw Hill, New York.

[8] White, Frank M., 1991, Viscous Fluid Flow, 2nd edition, McGraw Hill, New York.

[9] Coventry, J.S., 2002, Simulation of Concentrating PV/Thermal Collector Using TRNSYS, Solar Energy Conference 2002, Newcastle, Australia.

[10] Garg, H.P. and Adhikari, R.S., 1998, Transient Simulation of Conventional Hybrid Photovoltaic/Thermal (PV/T) Air Heating Collectors, Int. J. Energy Research 22, 547-562.

[11] http://solar.anu.edu.au

Reproduced with permission of the copyright owner. Further reproduction prohibited without permission.

VITA

Graduate College
University of Nevada, Las Vegas

Isaac Mahderekal

Home Address:
1305 E. Rawhide #106
Las Vegas, Nevada 89119

Degrees:
Bachelor of Science, Mechanical Engineering, 2002
University of Nevada, Las Vegas

Publications:
Mahderekal, R. F. Boehm, Thermal Analysis of a Concentrating Photovoltaic Receiver, Solar 2004 conference, Portland, Oregon.

Thesis Title: Thermal Analysis of a Concentrating Photovoltaic Receiver

Thesis Examination Committee:
Chairperson, Dr. Robert F. Boehm, Ph. D.
Committee member, Dr. Bingmei M. Fu, Ph. D.
Committee member, Dr. Woosoon Yim, Ph. D.
Graduate Faculty Representative, Eugene McGaugh, Ph. D.

Reproduced with permission of the copyright owner. Further reproduction prohibited without permission.